

Electronic Theses and Dissertations, 2004-2019

2014

Decentralized Power Management in Microgrids

Amit Bhattacharjee
University of Central Florida

 Part of the [Mechanical Engineering Commons](#)
Find similar works at: <https://stars.library.ucf.edu/etd>
University of Central Florida Libraries <http://library.ucf.edu>

This Masters Thesis (Open Access) is brought to you for free and open access by STARS. It has been accepted for inclusion in Electronic Theses and Dissertations, 2004-2019 by an authorized administrator of STARS. For more information, please contact STARS@ucf.edu.

STARS Citation

Bhattacharjee, Amit, "Decentralized Power Management in Microgrids" (2014). *Electronic Theses and Dissertations, 2004-2019*. 4591.
<https://stars.library.ucf.edu/etd/4591>

DECENTRALIZED POWER MANAGEMENT IN MICROGRIDS

by

AMIT KUMAR BHATTACHARJEE
B.E. Jadavpur University, 2008

A thesis submitted in partial fulfilment of the requirements
for the degree of Master of Science
in the Department of Mechanical and Aerospace Engineering
in the College of Engineering and Computer Science
at the University of Central Florida
Orlando, Florida

Fall Term
2014

Major Professor: Tuhin K Das

© 2014 Amit Kumar Bhattacharjee

ABSTRACT

A large number of power sources, operational in a microgrid, optimum power sharing and accordingly controlling the power sources along with scheduling loads are the biggest challenges in modern power system. In the era of smart grid, the solution is certainly not simple paralleling. Hence it is required to develop a control scheme that delivers the overall power requirements while also adhering to the power limitations of each source. As the penetration of distributed generators increase and are diversified, the choice of decentralized control becomes preferable. In this work, a decentralized control framework is conceived. The primary approach is taken where a small hybrid system is investigated and decentralized control schemes were developed and subsequently tested in a hardware in the loop in conjunction with the hybrid power system setup developed at the laboratory. The control design approach is based on the energy conservation principle. However, considering the vastness of the real power network and its complexity of operation along with the growing demand of smarter grid operations, called for a revamp in the control framework design. Hence, in the later phase of this work, a novel framework is developed based on the coupled dynamical system theory, where each control node corresponds to one distributed generator connected to the microgrid. The coupling topology and coupling strengths of individual nodes are designed to be adjustable. The layer is modeled as a set of coupled differential equations of pre-assigned order. The control scheme adjusts the coupling weights so that steady state constraints are met at the system level, while allowing flexibility to explore the solution space. Additionally, the approach guarantees stable equilibria during power redistribution. The theoretical development is verified using simulations in matlab simulink environment.

TABLE OF CONTENTS

LIST OF FIGURES	viii
LIST OF TABLES	x
CHAPTER 1: INTRODUCTION	1
CHAPTER 2: BACKGROUND AND RELATED WORKS	5
2.1 Classical Active and Reactive Power Control in Power System	6
2.2 Speed Droop and Active Power Management [33]	8
2.3 Voltage Droop and Reactive Power Management [33]	10
2.4 Voltage Source Inverters and Their Application on Microgrids	12
2.5 Distributed Generators and Impact on Microgrids	14
CHAPTER 3: PRIOR WORK ON DECENTRALIZED POWER MANAGEMENT OF HYBRID NETWORK	17
3.1 System Description	18
3.2 Control Objectives	20
3.3 Decentralized Power Management Using Energy Conservation	20

3.3.1	Approach	20
3.3.2	Robust Performance Through Dissipation	23
3.3.2.1	Design of K_1 Using a Lower Bound on η_2 and $\bar{\eta}_2$	23
3.3.2.2	Dissipation Based Design of K_2	24
3.3.3	Robustness through voltage modulation	27
CHAPTER 4: DETAILS OF PRACTICAL IMPLEMENTATION		30
4.1	Power Converter topologies	30
4.2	Control of Unidirectional Converter C_1	32
4.3	Bidirectional Converter Control	34
4.4	η_1 Measurement	34
4.5	PWM Switching Circuit	35
4.6	Experimental Results	38
4.6.1	Experimental Validation of Dissipative Method	38
4.6.2	Experimental Validation of Voltage Modulation	40
4.7	System Loss Comparison	42
4.8	Fault Tolerance Provisions in Decentralized Framework	44
CHAPTER 5: COUPLED DYNAMICAL SYSTEM APPROACH		46

5.1	System Description	48
5.1.1	Model Development	49
5.1.2	Mapping On to a Graph	50
5.2	Proposed Framework	51
5.2.1	Problem Formulation	52
5.2.2	Reverse Cholesky Factorization	53
5.2.3	Steady State Solution and Constraint	54
5.3	Decentralized Implementation	55
5.3.1	Linear Parameterization of a_{ij}	56
5.4	Stability	59
5.5	Structural Controllability	60
5.6	Lower Layer Operations	63
5.7	Simulation and Results	64
5.8	Overall Implementation In Power System	69
CHAPTER 6: CONCLUSION		73
APPENDIX : INPUT TO STATE STABILITY		74

LIST OF REFERENCES 76

LIST OF FIGURES

Figure 2.1:Real and reactive power flows[2]	7
Figure 2.2:Block Diagram of Speed droop control of generators [33]	8
Figure 2.3:Plot of Frequency vs Active power [33]	9
Figure 2.4:Plot of Voltage vs Reactive power [33]	11
Figure 2.5:General Structure of an inverter controlled Microgrid	13
Figure 2.6:General Structure of a microgrid [46]	15
Figure 3.1:Block Diagram representation of SOFC System	18
Figure 3.2:Schematic of Hybrid SOFC System with Decentralized Controller	19
Figure 3.3:Energy Conservation based Approach	21
Figure 3.4:Conservation of energy with a Conservative Estimate of η_2 and $\bar{\eta}_2$	24
Figure 3.5:Dissipation Circuit	25
Figure 3.6:System response with a PI controller for dissipation	26
Figure 3.7:Simulations with Voltage Modulation and Efficiency Estimation	28
Figure 4.1:two-quadrant Power converter topology	30
Figure 4.2:Power converter: Internal Control	31

Figure 4.3:Schematic of Signal Flow in K_1	33
Figure 4.4:Implementation of External Voltage Modulation on C2	34
Figure 4.5:(a) Schematic for PWM generator. (b) Discharge Circuit. (c) Gate Driver. (d) Switching Circuit.	36
Figure 4.6:Experimental Test Stand	36
Figure 4.7:Typical Dspace control panel during operation	38
Figure 4.8:Experimental Results for Dissipation Based Approach	39
Figure 4.9:Experimental Results for Voltage Regulation Based Approach	41
Figure 4.10Power Loss patterns with Voltage Regulation and Dissipation based framework	43
Figure 5.1:Two layer control structure	49
Figure 5.2:Mapped Graph	51
Figure 5.3:Decentralized Framework	64
Figure 5.4:Simulation Result for topology 1	66
Figure 5.5:Simulation Result for topology 2	67
Figure 5.6:Effect of varying topology	68
Figure 5.7:Inverter Control Scheme	70
Figure 5.8:Overall system diagram Combining power system layer and control layer	72

LIST OF TABLES

Table 4.1: Equipment specifications	37
---	----

CHAPTER 1: INTRODUCTION

In the rapidly changing Power grid operations, the integration of distributed generators to the power grid has become a much debated issue. A number of groups have tried to address this problem in significant details. Essentially, with the advent of Power Converter, controlling the out put voltage and frequency has become an achievable target. However, the practical application requires large number of power sources and loads to be interconnected and naturally the load sharing among them becomes a challenging task. Parallel operating sources are certainly a solution but with possibilities of power line disturbances and intermittent nature of most of the comparatively high yield renewable sources, makes a simpler paralleling ineffective. Naturally, separately controlling each of the inverter/sources in a parallel connected mode was developed in [2]. With these capabilities in the power layer of the grid, a sophisticated framework is required which will essentially determine the reference of the output power for each distributed generators(DG). In [1, 3], the author developed some effective power management strategies to control active and reactive powers in DGs both in autonomous and islanded mode. In [4],[5], the voltage and power angle droop has been utilized to make the control decentralized. Some load side management schemes were also been investigated [7], and secondary control were necessary to implement an intelligent control framework necessary for smarter grid operations. However all these control strategies are more or less non-flexible as integration of renewable sources brings in a factor of non-realiability in the system and droop methods cannot function effectively in case of source intermittency. Also, in the islanded mode of operation an additional communication is required for secondary control functions and power management,as described in [6]. In addition to this, the conventional control strategies may exhibit stability issues with high penetration of DGs as discussed in [9].

The control and stability of large networked system has drawn a lot of interest due to the wide application area, and requirement of proper control for the large system stimulated interest in distributed control in recent years. The implementation, cost and reliability of such systems are important aspect of consideration, and naturally, the decentralized control strategies emerges as a suitable candidate due to the size and the complexity of such systems along with the difficulties in controlling them. A detailed description of such complex systems is given in [71]. The core challenges are dimensionality, information structure constraints, uncertainty and delay. Related work on decentralized stabilization of interconnected dynamical systems appears in [69, 70]. Decentralized control on power grids as a complex large scale dynamical system appears in [64, 65], where the authors address robust stability of large-scale power systems. On the other hand, operating such large scale systems is also required to be fault tolerant and reliable. To address that, the issue of cascaded tripping in power networks can be dealt with a decentralized architecture given in [66]. In [67], a novel decentralized fault tolerant control structure was developed using droop control. Additionally, to mitigate cascaded failures in large power network, multi-agent based decentralized control using a novel optimization framework can be found in [68].

Advancements in multi-agent systems and distributed control strategies along with advanced optimization frameworks addresses the dynamics of electricity market as well as the optimal scheduling approach as described in [7],[8], whereas some research efforts were dedicated towards the transient stability of the system and optimal load dispatch using cooperative control methods and game theory approach in [10],[11]. Also, some LQR based design on synchronicity of networked system has been studied in [10] . However, these frameworks are inherently leader-follower type, which require selection of leader agents and that brings in the task of maintaining reliability of the leader node. However that may not always be practically possible and cost effective.

Therefore a more flexible framework with each control points enjoying an equal importance was required for stable operation of microgrid [17] both in grid connected and islanded mode of operation, and that too in decentralized fashion. In this work, we look at a much simpler and scaled down version of the problem at first and try to address the decentralized control aspect of the problem using conservation of energy principle on a small hybrid power system consisting of a fuel cell and an ultra-capacitor. With the progress of the work, we look for a more rigorous and scaled up version of the problem where a large number of sources can be integrated to the grid. Here the control system itself has been treated as a set of coupled autonomous systems. The interaction between the autonomous systems has been made modulating so that the equilibrium point can span across a defined possibility region. Also, efforts have been made to simultaneously reduce the amount of interaction between the nodes and still achieve the same performance. Frequently, the system has been referred through an equivalent graph, however the analysis has mainly been done using systems theory. Only to demonstrate the physical variation of the system parameters and the effect of the interconnections, a graphical portrayal of the system is presented. Linking back to the micro grid discussion, the main objective of the work is decided to be the effective load sharing between DGs in steady state condition, also assumption has been made on the sufficiency of the storage/reactive elements of the power system to take care of the voltage stability issues.

The framework directly controls the inverters connected to the grid or synchronous generators with active/reactive power control loop which forms the power system layer, although an effort has been made to present the work in general terms in its design phase, so that it can be equally applied to any distributed system.

Following chapter encompasses the general structure of a power grid and existing strategies of active and reactive power control. We will look into greater details of the application

of sophisticated controllers on smart grid application. Following that we will introduce the prior works that were done on a small scale equivalent of the grid which entails conceptual development of the controller and verification through simulation. Following that we discuss the experimental verification of the energy conservation based framework on a laboratory prototype. In the next chapter we introduce the novel framework for controlling the active power based on coupled autonomous system theory followed by a complete description of power flow controllers on a power grid and simulation results.

CHAPTER 2: BACKGROUND AND RELATED WORKS

Power network being the oldest and most reliable machine ever built by humans, stood strong against the flow of time and continued to provide quality electricity. However, with the modernization of society the demand and quality requirements of consumable electricity has been increased significantly. To cater to the growing need of power quality and reliability, a 'smarter grid' is envisioned. The formal definition of smart grid is to couple the communication and cyber-physical system to the more rudimentary power network and achieve a more developed grid system which simultaneously control the power flow depending on real time power market scenarios, outage status, network configuration and the transient load variations[62]. A no of sophisticated approaches were proposed for the challenging task of the power control with so many different aspects taken into configuration. Naturally, in the present time of modernization and pinnacle of technological advancements, no straight forwards source-load concepts dominate the powergrid, instead, with the advent of hybrid electrical vehicle and concept of self sustaining energy sources, such as UPS (Uninterruptible Power Supplies) [25] prevails. Therefore, treating each control points of the network as of same generic characteristics, and yet designing a control system that addresses all possible control problem that may arise in different situation, is quite a challenge. Also, the growing need for integrating renewable energy sources into the grid, comes with a challenging task of accommodating all the inherent intermittency [26, 27] and non-reliable nature [28] of some of these renewable and non-conventional sources. In this chapter we shall revisit some of the existing classical approaches in existence for controlling the power flow in the network, then we will gradually transcend to the modern approaches undertaken in order to improve the load sharing problem.

2.1 Classical Active and Reactive Power Control in Power System

The control of frequencies in power grid operations are critical, and it influences the active power control of the power grid as well as the steady state stability. Similarly the voltage control of the network influences the reactive power control and vice versa. Tight control of the frequency ensures the constancy of the speed of motor drives for induction and synchronous motors connected to the network and it is very important for proper functioning of the generators as they are highly dependent on the auxiliary drives used in different aspects starting from fuel mass flow rate to feed-water and combustion of air supply. Also, motors used in industry comes with a drives calibrated for a set power frequency, and hence proper functioning of all industrial motors highly depends on the system frequency. The frequency and the speed of the synchronous generator is related as

$$f = \frac{pn}{120} \quad (2.1)$$

where, p is the number of pole pairs and n is the speed of the machine in r.p.s. Again, the active power of the machine is given as

$$p = T_{eff} \omega_m \quad (2.2)$$

whre T_{eff} is the effective applied torque at the prime mover after considering the mechanical losses, and ω_m is the mechanical speed of the rotor, which can be found from the r.p.s speed mentioned before as,

$$\omega_m = \frac{n}{2\pi} \quad (2.3)$$

therefore controlling the frequency, the active power can be controlled effectively. The active power and reactive power of a network can be expressed as following [2] and [33]

$$P = \frac{V}{\omega} \frac{E}{L_f} \sin \delta \quad (2.4)$$

and

$$Q = \frac{V^2}{\omega L_f} - \frac{VE}{\omega L_f} \cos \delta \quad (2.5)$$

where ω is the electrical speed of the machine, P and Q are the active and reactive powers flowing through the network, L_f is the inductive reactance or inductance of the transmission line (which is assumed to be predominantly inductive, as it is in the practical scenario). V and E are the voltages at the source and receiving end. A quick illustration of the system is given in the following figure.

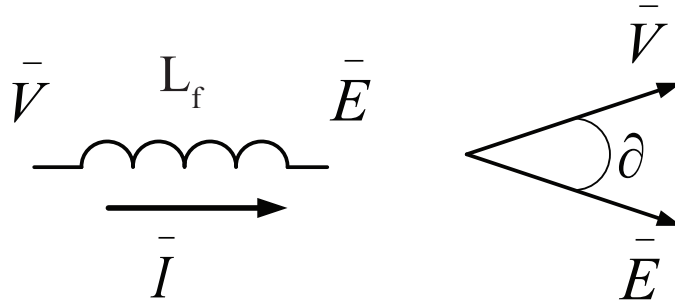
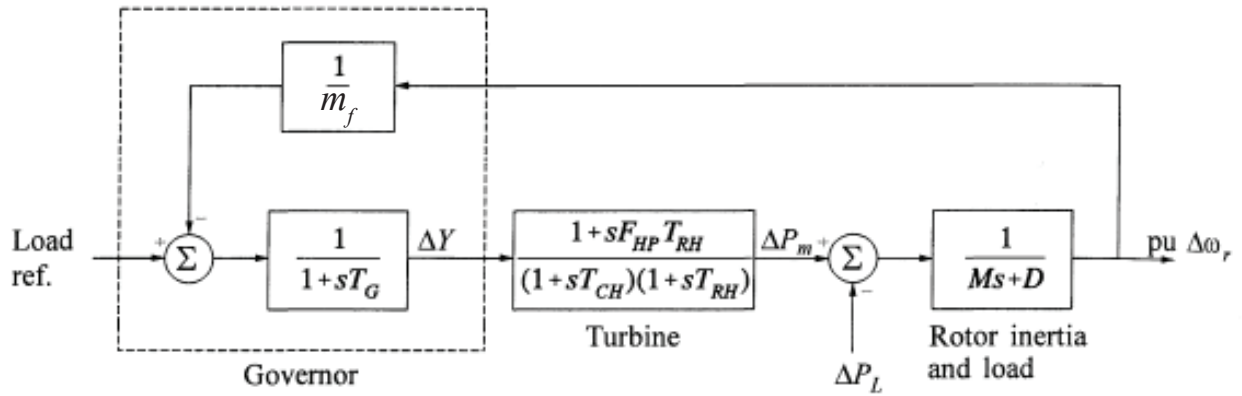


Figure 2.1: Real and reactive power flows[2]

2.2 Speed Droop and Active Power Management [33]

Speed droop control strategy is a very reliable method to control the frequency of the grid by controlling the speed of the generators. In case of conventional synchronous governors[33], the speed regulation can be represented by the following block diagram, details of which can be found in the cited text.



Typical values:

$$\begin{array}{llll}
 m_f = 0.05 & T_G = 0.2 \text{ s} & F_{HP} = 0.3 & T_{RH} = 7.0 \text{ s} \\
 T_{CH} = 0.3 \text{ s} & F_{LP} = 0.7 & M = 10.0 \text{ s} & D = 1.0
 \end{array}$$

Figure 2.2: Block Diagram of Speed droop control of generators [33]

Where a typical droop of m_f has been introduced where m_f is percent speed regulation or the droop. The graphical representation of the m_f has been depicted in the picture follows.

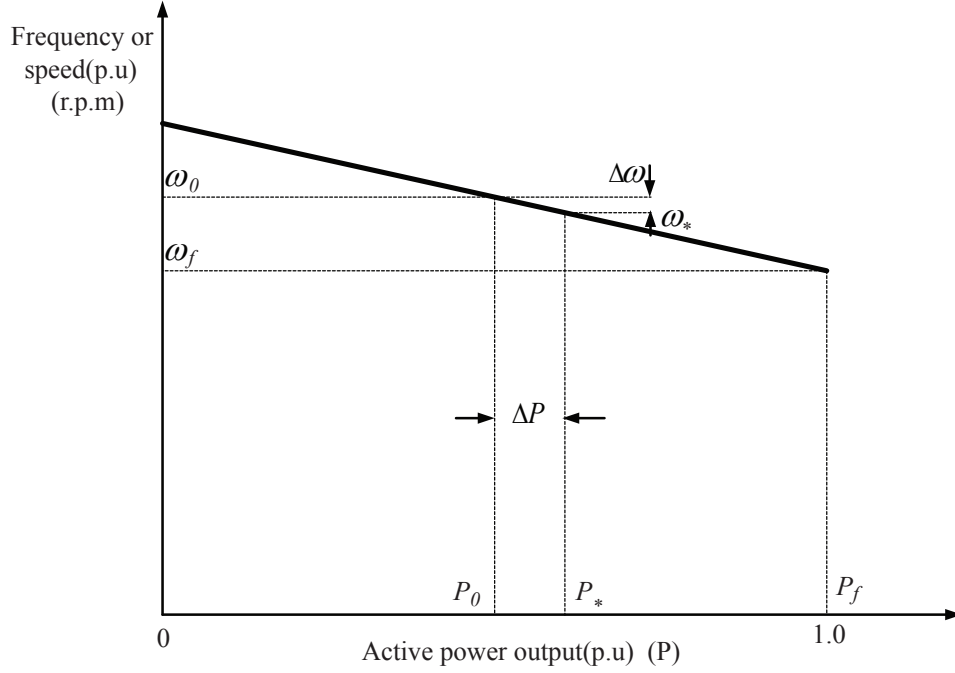


Figure 2.3: Plot of Frequency vs Active power [33]

Therefore, as the regulation index m_f effectively describes the slope of the speed droop curve, it is quite standard to use a speed droop curve to regulate the active power out put of the generator.

Mathematically, the speed droop control can be represented as follows,

$$f_* = f_0 + m_v(P_* - P_0) \quad (2.6)$$

$$m_f = \frac{f_f - f_0}{P_f - P_0} \quad (2.7)$$

In the context of microgrid operation, active power control is a very important issue, where grid synchronization is not available in certain mode of operation (e.g. islanded mode). However, the droop control method has been extensively used here for normal mode of operations, [29, 30, 31, 32]. Electronically interfaced power sources such as inverter controlled renewable sources were also reported to be effectively controlled using droop control method in [1, 3]. Whereas control parallel inverter control for a stiff ac system using droop principles were presented in [2, 4]. A detailed comparison of the variations of the speed droop curve and their effectiveness on active power management are detailed in [47].

2.3 Voltage Droop and Reactive Power Management [33]

As equally important as the active power counterpart, the reactive power of a network plays a very important role in transient stability of the system. Similar to the speed droop control in case of active power management, a voltage versus reactive power droop curve (fig. 2.4) is used for regulation of the voltage across the generator.

Mathematically, the voltage droop control can be represented as follows,

$$V_* = V_0 + m_v(Q_* - Q_0) \quad (2.8)$$

$$m_v = \frac{V_f - V_0}{Q_f - Q_0} \quad (2.9)$$

where m_v is the slope of the voltage droop curve.

However, the generating unit provides the primary means of control; however, as typically the grid spans across a huge geographical area and therefore it is unavoidable to have large

transmission lines joining the source to load. This additional element of the network causes power losses over the network and the voltage at different points of the network is usually at different voltage levels, and hence to improve the quality of power over the network, static VAR compensators (SVC) are used[33]. Also, static shunt/series capacitors, shunt/ series reactors are frequently used to maintain voltage in the transmission and distribution lines [33, 54] and in [55].

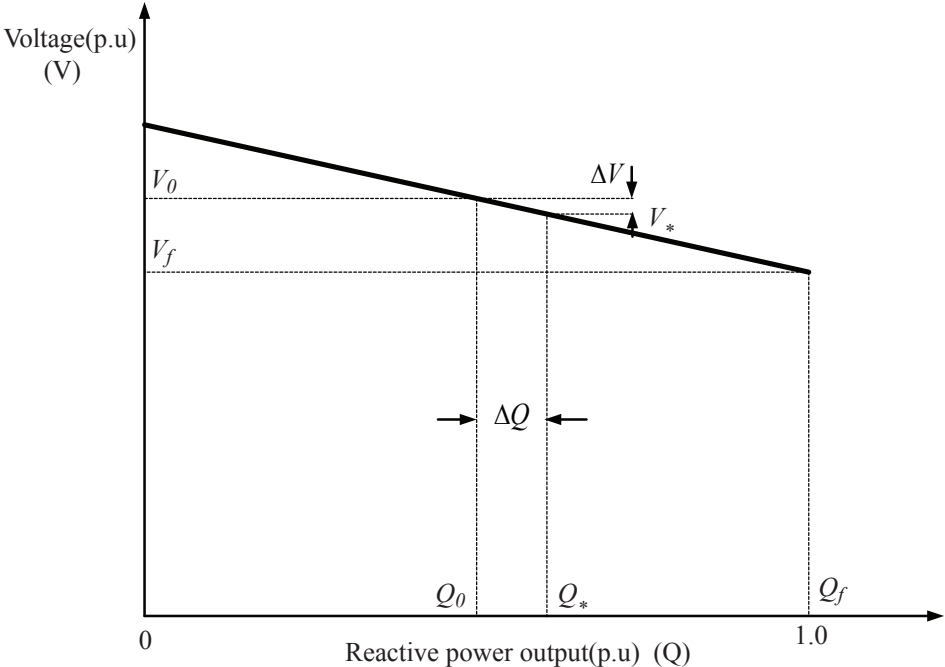


Figure 2.4: Plot of Voltage vs Reactive power [33]

In [51], the voltage rise induced by the active power variation is shown to be controlled by appropriately tuning the reactive power output at the generator terminal without changing the power factor too much, shown to be an improvement over the lag/lead power factor control. However Distribution Network Operator(DNO) practices on-load tap changer in distribution

transformer to mitigate voltage rise issues depicted in [52]. The new improvements in voltage rise mitigation in [51] is effective in conventional power grid, however with high penetration of DGs and electronically interfaced power sources or inverter based distributed power generation requires more sophisticated control design. In [53], a reactive power injection based control was described which shown to be effectively control inverter based DGs.

2.4 Voltage Source Inverters and Their Application on Microgrids

Voltage source inverters (VSIs) have been used as an essential means of power conversion for better control and reliability purposes. Extensive discussion on the structure and working principles of a VSI can be found in [25]. Application of VSIs in microgrid distributed generation has been a wide spread trend because the enabling technology VSIs provide to implement advanced control systems. In works [2, 34, 35], several different current, voltage, active or reactive power control strategies are described for wide application areas such as motor drives, grid applications etc. Some more advanced control techniques used in works [36, 37] to further improve the performance of the converter. Cascaded PI control loops were implemented in [39] in order to use VSI in a microgrid environment.

Numerous power management strategies have been developed with inverter controlled DG units in a microgrid, the details of which can be found in [1]-[5]. The core power management strategy is often droop based control[1, 2, 3], however some other interesting solutions have been suggested in [21, 29, 32, 34]. A detailed block diagram representation of a inverter controlled DG power management can be found in the fig.(2.5).

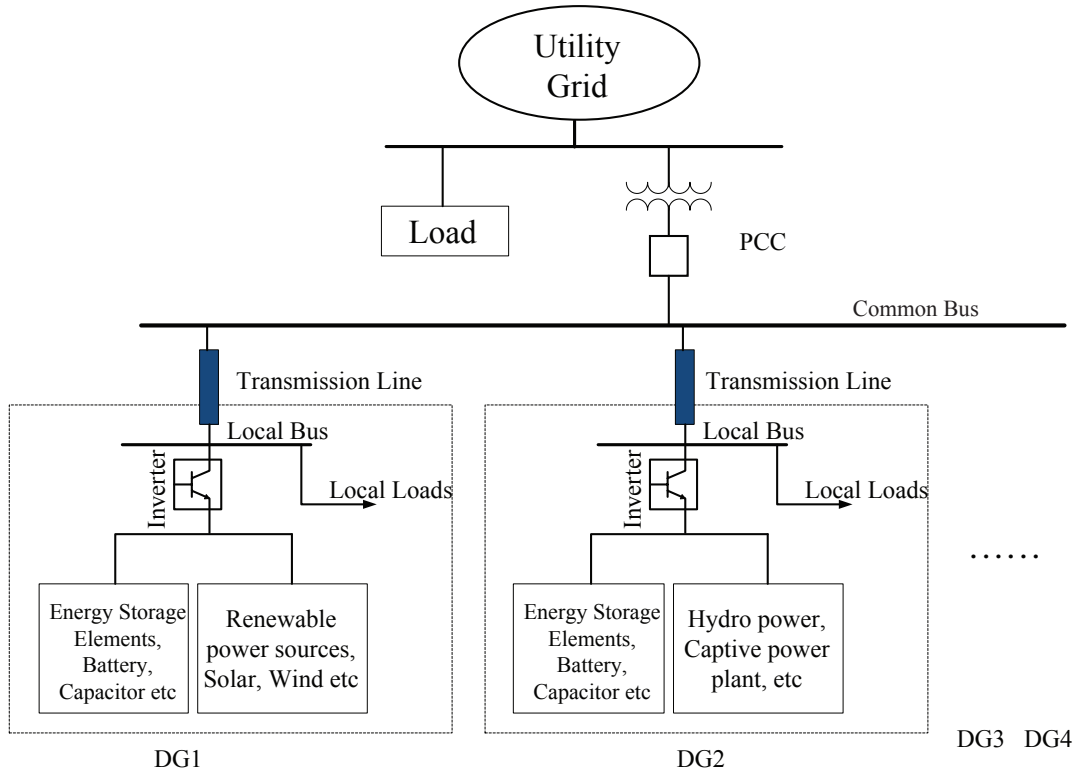


Figure 2.5: General Structure of an inverter controlled Microgrid

The point of common coupling (PCC) signifies the coupling point of the microgrid with the larger grid. The main utility grid supplies a portion of the total load on the grid and also provides/receives power from each of the microgrid connected to it through the PCC. Also, each of the DGs shown in the figure are connected to the PCC as well as to the utility grid through inverters. Additional reactive power support has been provided by implementing energy storage element to the DGs. Similar approaches can be found in [1, 3].

2.5 Distributed Generators and Impact on Microgrids

With the modernization of the power grid and more integration of the renewable energy sources have become a preferred choice, especially since the growing concern for carbon footprint which is increasing with fossil fuel based power generation systems. Renewable sources provide clean and sustainable source of energy, and naturally is preferred over the thermal energy counterpart. However, integration of renewables poses a challenging task as often the renewable sources are dependent on natural processes and therefore are geographically sparse and non-flexible in terms of its operation capability. Therefore this distributed generators, in order to integrate to the larger grid, needs proper means of integrating devices and sophisticated control methodologies. A voltage source inverter(VSI) is one of the best choices available to integrate distributed resources to the grid, However the power management between several distributed generators connected to the grid via VSCs is quite a challenge as many researchers over the years attempted to formulate good power management strategies. In the following subsections, a brief discussion about the architecture and control of voltage source converters will be discussed which will be followed by a discussion on the presently available power management strategies and their merits and demerits on the larger context of grid operation.

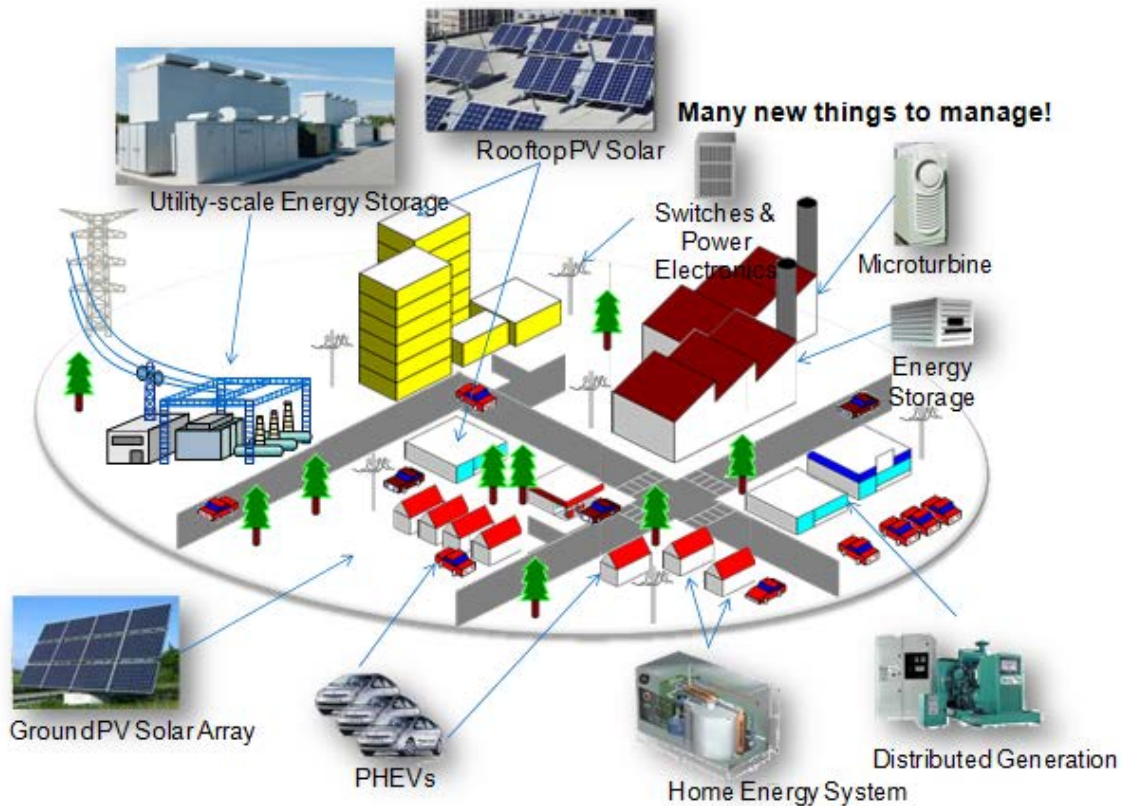


Figure 2.6: General Structure of a microgrid [46]

Many research groups have also worked on the transient stability of the microgrid in great details and have pointed out the influence of the distributed generation on the microgrid [48, 49] which talks about planning tools and general conclusion on the stability issues with high penetration of DGs into a microgrid. However problems associated with high penetration of DGs are discussed in [50] and in [51]. As discussed previously, the voltage control issues typically contribute to the transient stability of the grid and the active power control ensures the demand-supply and the network quality and reliability issues. With

the proliferation of smart operation of microgrids with the integration of renewable energy sources and inverter based DGs, significant research efforts were made in [1]-[11]. With a combined system of energy storage elements and the inverter controlled DGs with proper control strategies, the smart operation can be performed in a microgrid as proposed in [10, 11, 12, 16, 22, 57], using a cooperative control approach. Also numerous other control strategies are proposed for the power management of a power grid or micro grid in works [1]- [7]. However as the size of the grid increases the complexity associated with designing the proper control framework increases as well. Multi-agent based control structure has gained quite popularity recently [12, 58, 59]. Although cooperative and multi agent based control of power flow brings in an exciting and new perspective to the problem, they are often optimization based approaches[10, 11, 12, 60] and complexity of the computation is very high which requires high end computation power and resources, and the complexity progressively increases with the increase of the network size. Therefore this necessitates a much simpler and easy to implement control framework that effectively addresses all the control problem posed and requires much less computation power. With the existing pool of resources, we look for a novel control framework to control the power flow in a microgrid.

CHAPTER 3: PRIOR WORK ON DECENTRALIZED POWER MANAGEMENT OF HYBRID NETWORK

With the backgrounds and related works outlined in the previous section, we started formulating the power flow control or the load sharing control problems in a multi DG microgrid. Since a modern power system scenario has been assumed, for smart operation of the system, every limitations of each of the component and the overall system is required to be kept in mind.

In works [61] and in [62], the guidelines about the smart operation of a power grid is discussed. The preserving of assets by not going beyond the absolute current or voltage or power limits of equipment, maintaining a secondary control over each DGs so that an emergency shutdown may be applied in the event of a failure, fault tolerant operation of power sources or catering to any local disturbances with out affecting the larger grid operation are one of the most important constraints to e addressed while supplying the demanded power from the utility grid. The first steps in achieving that goal are essentially modeling a smaller part of the microgrid along with its constraints as discussed and try to develop a control algorithm that addresses them all while successfully supplying the demanded quality power. In an attempt to develop small scale power system we choose a hybrid power network representing a very small version of the larger microgrid. It consists of a power source, a solid oxide fuel cell(SOFC) and a storage element, an Ultra-capacitor. Following discussions will describe the structure of the system in consideration and the control algorithm developed to control it in a decentralized manner.

3.1 System Description

The SOFC system considered in this work is depicted in Fig.3.1 and is identical to that developed and discussed in [41] and [42]. Details are omitted for brevity.

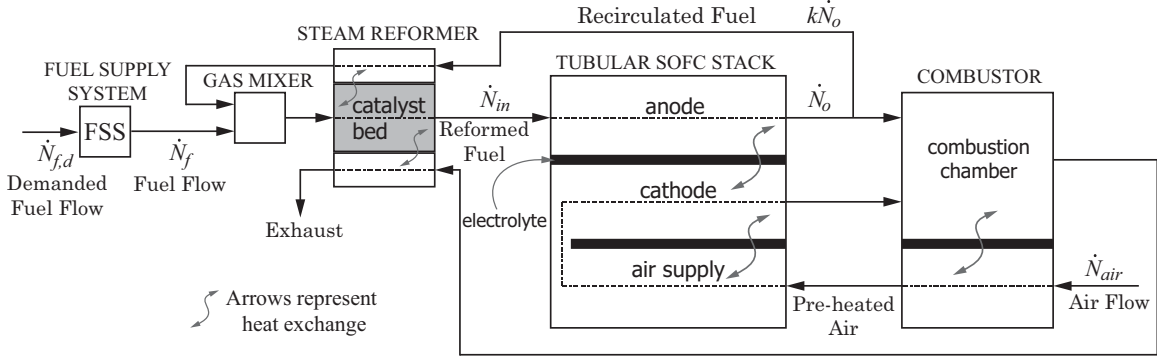


Figure 3.1: Block Diagram representation of SOFC System

Fig.3.2 demonstrates a schematic of the hybrid system with a decentralized control scheme. Other approaches for building a fuel cell ultra-capacitor/battery are presented in [43, 44]. In our approach, the fuel cell and the ultra-capacitor are connected in parallel. The fuel cell supplies power to the load through a uni-directional DC/DC converter C_1 . The ultra-capacitor is connected to the load through a bi-directional DC/DC converter C_2 allowing charge and discharge. Due to their fast responses, C_1 and C_2 are assumed to be static energy conversion devices, with C_1 having an efficiency of η_1 and C_2 having discharge and charge efficiencies of η_2 and $\bar{\eta}_2$ respectively [42]. We also assume that $\eta_{2,min} \leq \eta_2, \bar{\eta}_2 \leq \eta_{2,max}$.

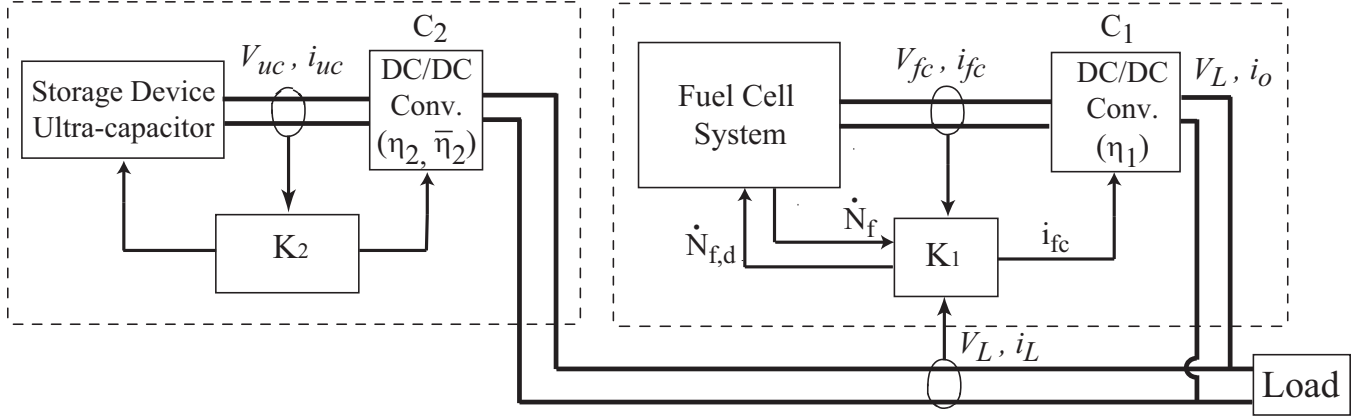


Figure 3.2: Schematic of Hybrid SOFC System with Decentralized Controller

From the schematic in Fig.3.2, since the fuel cell and the ultra-capacitor are connected in parallel, the following is true at all times:

$$V_L i_L = \eta_1 V_{fc} i_{fc} + \left[\frac{\eta_2 + \bar{\eta}_2}{2} + \frac{\eta_2 - \bar{\eta}_2}{2} \text{sgn}(i_{uc}) \right] V_{uc} i_{uc}, \quad (3.1)$$

To control both the voltage across and current through the load, we apply current mode controllers on C_1 and voltage mode controllers on C_2 to maintain a constant V_L across load.

Note: Since there is a reversal of power flow direction during charge and discharge of the ultra-capacitor, for discharge, η_2 is bounded by, $0 < \eta_2 < 1$ while for charging, $\bar{\eta}_2$ is bounded by, $\bar{\eta}_2 > 1$. This can be explained intuitively if the power input-output relation of C_2 is considered.

3.2 Control Objectives

Referring to Fig.3.2, the control objectives are:

1. **Power demand:** The net power demand $V_L i_L$ should be met by the hybrid power system at every instant.
2. **Fuel utilization:** The target fuel utilization at steady state will be $U_{ss} = 0.8$ while the deviations from U_{ss} during transients should be minimized [41, 42].
3. **SOC (State-Of-Charge):** Control scheme is designed to maintain the SOC of the ultra-capacitor at the target value of S_t .
4. **Decentralized controllers:** Design K_1 and K_2 (referring to Fig.3.2) with no mutual information sharing.

To realize a decentralized control, we impose the following restrictions on K_1 and K_2 . Controller K_1 can use measurements of V_{fc} , V_L , i_L and η_1 . However, it does not have measurements of i_{uc} , V_{uc} or η_2 . It commands C_1 to draw i_{fc} . Controller K_2 measures V_{uc} , i_{uc} , but does not have measurements of i_{fc} , V_{fc} , V_L , i_L or η_1 . K_2 commands C_2 to maintain a desired V_L .

3.3 Decentralized Power Management Using Energy Conservation

3.3.1 Approach

This work applies conservation of energy to develop decentralized control of the hybrid system in Fig.3.2. Conceptually, the approach is illustrated in Fig. 3.3.

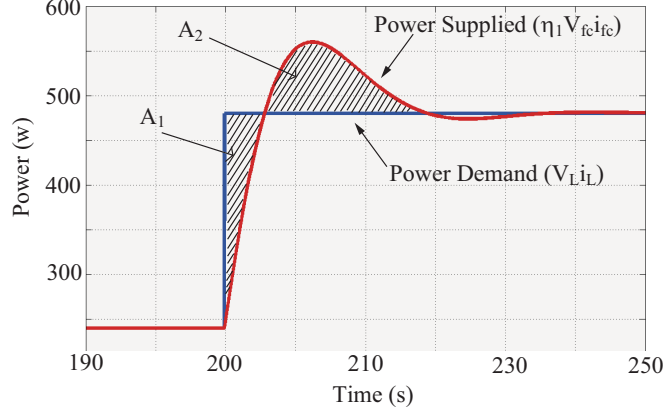


Figure 3.3: Energy Conservation based Approach

The figure shows a step change in power demand and the corresponding load-following response of the source (fuel cell). The area A_1 represents the energy supplied by the storage device (ultra-capacitor in this case) to make up for the fuel cell's deficiency for load following. Therefore, if the area A_2 , which represents the extra energy supplied by the source, is same as A_1 , that ideally charge the capacitor to its original SOC. Extending this idea, we note that if $\sum_i A_{1,i} = \sum_k A_{2,k}$, i.e. if

$$\lim_{t \rightarrow \infty} E_A = \lim_{t \rightarrow \infty} \left(\sum_i A_{1,i} - \sum_k A_{2,k} \right) \rightarrow 0 \quad (3.2)$$

then the storage element will maintain its original energy level. Ideally, the above condition can be satisfied by K_1 without any information about the capacitor by just ensuring

$$\lim_{t \rightarrow \infty} \int_0^t \Delta P dt = 0, \quad \Delta P \triangleq (V_L i_L - \eta_1 V_{fc} i_{fc}) \quad (3.3)$$

In the presence of losses in C_2 with discharge and charge efficiencies η_2 and $\bar{\eta}_2$ respectively,

Eq.(3.2) is modified to

$$\lim_{t \rightarrow \infty} E_A = \lim_{t \rightarrow \infty} \left(\sum_i \frac{A_{1,i}}{\eta_2} - \sum_k \frac{A_{2,k}}{\bar{\eta}_2} \right) \rightarrow 0. \quad (3.4)$$

If we assume η_2 and $\bar{\eta}_2$ to be known then, using ΔP as defined in Eq.(3.3), Eq.(3.4) is satisfied by K_1 by ensuring

$$\lim_{t \rightarrow \infty} I_e = 0, \quad I_e \triangleq \int_0^t \left[\frac{\eta_2^{-1} + \bar{\eta}_2^{-1}}{2} + \frac{\eta_2^{-1} - \bar{\eta}_2^{-1}}{2} \text{sgn}(\Delta P) \right] \Delta P dt \quad (3.5)$$

To demonstrate that conservation of energy approach can be used in principle to design decentralized control, we consider a simplified scenario. Assuming that in addition to the local information mentioned in Assumption 2, controller K_1 has exact knowledge of η_2 and $\bar{\eta}_2$. Next, in designing K_1 , we recall that the commanded i_{fc} must be based on the actual fuel flow \dot{N}_f for transient control of U , as detailed in [41]. Also, \dot{N}_f is driven by the demanded fuel $\dot{N}_{f,d}$, which in turn is determined from $i_{fc,d}$. Thus, the command i_{fc} to C_1 can be determined as:

$$\dot{N}_{f,d} = \frac{i_{fc,d} \mathcal{N}_{cell}}{4nFU_{ss}} \beta \Rightarrow i_{fc} = \frac{4nFU_{ss} \dot{N}_f}{\mathcal{N}_{cell} \beta}, \quad (3.6)$$

where $\beta = [1 - (1 - U_{ss})k]$. From Eq.(3.6) it can be noted that designing K_1 reduces to the design of the reference $i_{fc,d}$. The design of $i_{fc,d}$ is based on the following observation: In load-following mode, the fuel cell provides the entire power demand at steady-state and uses transient perturbations in power to regulate the ultra-capacitor SOC. With this goal, and incorporating the approach outlined in section 3.3.1, we formulate $i_{fc,d}$ as:

$$i_{fc,d} = \frac{V_L i_L}{\eta_1 V_{fc}} + k_i I_e, \quad k_i > 0 \quad (3.7)$$

where I_e is defined in Eq.(3.5). This design is implemented and simulation results are

summarized in Fig.3.4. The parameter values chosen are

$$C = 25F, \eta_1 = 0.8, \eta_2 = \bar{\eta}_2 = 0.8, k_i = 0.01 \quad (3.8)$$

The power demand $V_L i_L$ is subjected to step changes. We note that K_2 simply maintains the constant voltage V_L across the load. However, η_2 and $\bar{\eta}_2$ will be unknown to K_1 . Therefore, we need to build a robust control around this principle to handle the uncertainty in a decentralized manner. The next section will demonstrate the validity of the main principle.

3.3.2 Robust Performance Through Dissipation

3.3.2.1 Design of K_1 Using a Lower Bound on η_2 and $\bar{\eta}_2$

Considering a more realistic case where K_1 has no information of η_2 and $\bar{\eta}_2$ but only knows a lower bound $\eta_{2,min} \leq \eta_2, \bar{\eta}_2$. Accordingly, in Eq.(3.7), instead of using I_e from Eq.(3.5), a conservative I_e is used:

$$I_e \triangleq \int_0^t \left[\frac{\eta_{2,min}^{-1} + \eta_{2,min}}{2} + \frac{\eta_{2,min}^{-1} - \eta_{2,min}}{2} \text{sgn}(\Delta P) \right] \Delta P dt \quad (3.9)$$

It can be observed that Eqs.(3.6), (3.7) and (3.9) together generate a feedback loop. This is because the FSS dynamics, considered nonlinear and unknown, relates i_{fc} to $i_{fc,d}$ through a general form

$$\frac{di_{fc}}{dt} = f(i_{fc}, i_{fc,d}), \quad \text{such that} \quad \lim_{t \rightarrow \infty} i_{fc} = i_{fc,d}. \quad (3.10)$$

It is evident from Eqs.(3.7) and (3.9) that for a step change in i_L , $\lim_{t \rightarrow \infty} \Delta P = 0$. Moreover, since $\Delta P = i_L V_L - \eta_1 V_{fc} i_{fc}$, hence from Eqs.(3.10), $\lim_{t \rightarrow \infty} i_{fc,d} = i_{fc} = i_L V_L / \eta_1 V_{fc}$ and that $\lim_{t \rightarrow \infty} I_e = 0$. We omit formal stability proof for brevity.

Simulation results with I_e calculated using Eq.(3.9) are shown in Fig.3.4. The parameter values chosen were same as in Eq.(3.8). Additionally, $\eta_{2,min} = 0.7$ was chosen.

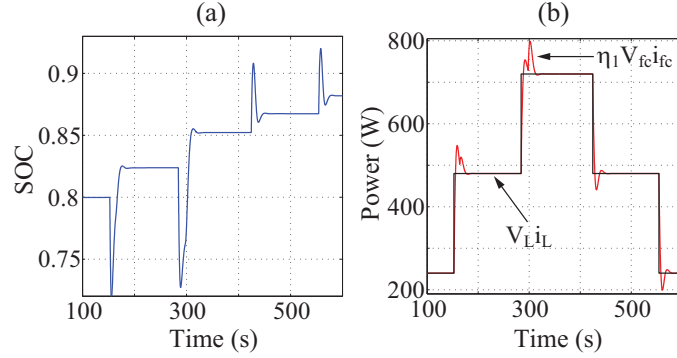


Figure 3.4: Conservation of energy with a Conservative Estimate of η_2 and $\bar{\eta}_2$

The formulation of I_e according to Eq.(3.9) is conservative since it always overestimates and underestimates the energies from and to the capacitor respectively. The conservative nature of this approach can be inferred from Fig.3.4(a) where the SOC builds up with changes in power demand. The power demanded and power supplied are plotted together in Fig.3.4(b). Since the ultracapacitor is of finite capacity, one must regulate the SOC. To address this in a decentralized manner we design dissipation based controller K_2 .

3.3.2.2 Dissipation Based Design of K_2

In this approach, the ultra-capacitor's SOC is regulated via dissipation through a variable resistance. We choose to add a resistance in parallel with capacitor which is shown in Fig.3.5. Energy dissipation is controlled by K_2 by actuating a pulse-width-modulated switch S_1 , shown in Fig.3.5. Since the SOC is a local information for K_2 , charge management is done locally without any information about the fuel cell from K_1 .

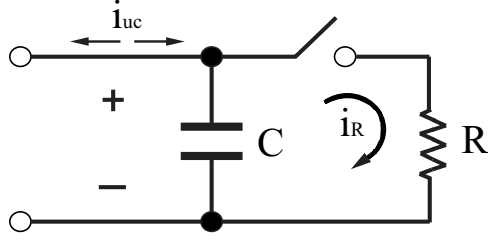


Figure 3.5: Dissipation Circuit

The circuit equation corresponding to Fig.3.5 is:

$$C\dot{V}_{uc} = -(i_{uc} + i_R), \quad \dot{V}_{uc} = -\frac{1}{C}(i_{uc} + V_{uc}\sigma_R) \quad (3.11)$$

where σ_R is the effective conductance that can be varied by changing the duty cycle of S_1 .

We treat σ_R as a control input and use the following control law to stabilize the equilibrium

$$V_{uc} = V_{uc,d}$$

$$\sigma_R = \frac{k_{p,uc}}{V_{uc}}(V_{uc} - V_{uc,d}) + \frac{k_{i,uc}}{V_{uc}} \int_0^t (V_{uc} - V_{uc,d}) dt, \quad \begin{cases} \dot{\sigma}_R = 0, & \text{if } \sigma_R = \sigma_{R,max} \text{ and } V_{uc} > V_{uc,d} \\ \sigma_R = \dot{\sigma}_R = 0, & \text{if } V_{uc} \leq V_{uc,d} \end{cases} \quad (3.12)$$

where $V_{uc,d}$ is such that $V_{uc,d}/V_{uc,max} = S_t$, the target SOC. The efficacy of this controller is shown through the simulation results in Fig.3.6. The manner in which the resistance R is used in the PI control is evident from Fig.3.6(b). For this simulation, $S_t = 0.8$ and $V_{uc,max} \approx 16V$, and hence $V_{uc,d} = 13V$. Also, $k_{p,uc} = 0.08$ and $k_{i,uc} = 0.0016$. We assume $R = 25\Omega$, and that σ_R varies linearly with from duty cycle = 0 $\Rightarrow \sigma_R = 0$, to duty cycle = 1 $\Rightarrow \sigma_R = 0.04$.

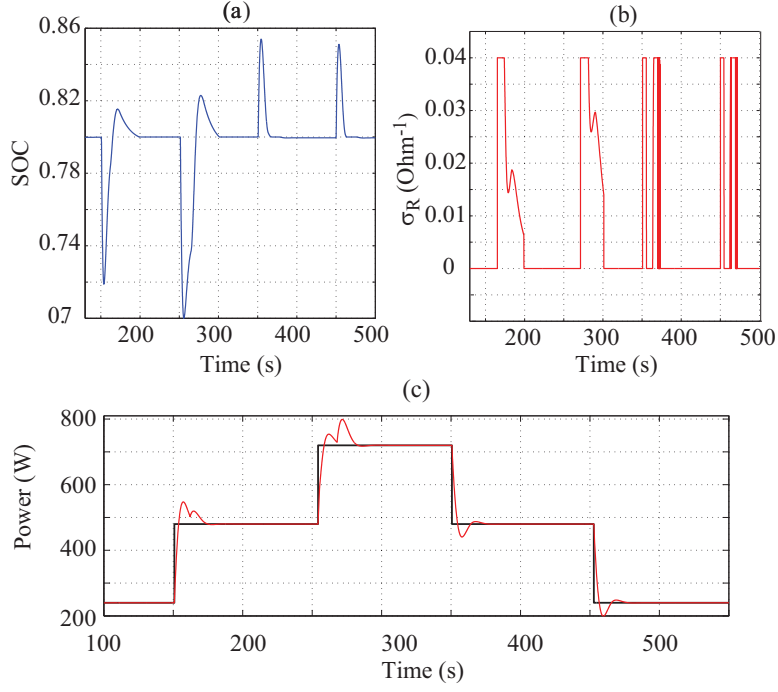


Figure 3.6: System response with a PI controller for dissipation

In contrast to Fig.3.4(a) where the SOC control was not implemented in K_2 , the SOC converges to 0.8 with the control law of Eq.(3.12).

Note that in Eq.(3.12), we did not incorporate i_{uc} in the feedback although it is a local information. The reason is that we want σ_R to respond only to gradual (i.e. low frequency) changes in V_{uc} and not respond to high frequency components of V_{uc} or perturbations in i_{uc} . The current i_{uc} can be considered as a disturbance in Eq.(3.11). In load-following mode, i_{uc} would be close to zero and hence the noise-to-signal ratio of its measurement is expected to be high, especially when load variations are gradual. Since the change in SOC is expected to be a gradual process, we want σ_R to respond only to the low frequency component of V_{uc} . It is expected that the frequency content $\Omega_{i_{uc}}$ of i_{uc} to consist of that of i_L and that of i_{fc} . This is evident from Eq.(3.1). Considering a controller $D(s)$ connected in series to the plant

$G(s) = -1/(Cs)$ and a standard negative feedback loop, one can write

$$E(s) = \frac{1}{1 + L(s)}V_{uc,d}(s) + \frac{G(s)}{1 + L(s)}i_{uc}(s), \quad E(s) = V_{uc,d}(s) - V_{uc}(s), \quad L(s) = D(s)G(s) \quad (3.13)$$

where, the control input is $i_R = V_{uc}\sigma_R$. Since $V_{uc,d}$ is a constant, reference tracking and disturbance rejection can be simultaneously achieved by the PI controller proposed in Eq.(3.12), which translates into $D(s) = (k_{p,uc} + k_{i,uc}/s)$ in frequency domain. With this configuration, the loop gain $L(s)$ is high at low frequencies and low at high frequencies. Moreover, the zero at $(-k_{i,uc}/k_{p,uc})$ can be tuned to obtain a desired high frequency roll off. Furthermore, attenuation of i_{uc} is achieved at low frequencies due to $|L(j\omega)| \gg |G(j\omega)|$, and at high frequencies due to $|G(j\omega)| \rightarrow 0$.

3.3.3 Robustness through voltage modulation

Using dissipation based approach a fixed amount of energy is generally lost every time a load perturbation appears. The idea in the voltage regulation method is to minimize this loss. Evidently, energy loss would be prevented if the fuel cell controller K_1 has accurate knowledge of η_2 and $\bar{\eta}_2$. Hence, the objective of this design is to develop a mechanism by which K_1 can learn the aforementioned efficiencies without direct sensing or communication with K_2 . To this end, we propose the following approach. As mentioned in section 3.8, K_2 can manipulate V_L . Therefore K_2 can manipulate V_L based on the SOC of the ultra-capacitor. As the SOC deviates from the target S_t , V_L can be varied gradually by K_2 . Not only will it regulate V_{uc} , but since V_L is a global variable, the fuel cell can simultaneously use V_L to improve its lower bound $\eta_{2,min}$. The process, if designed properly, will cause $\eta_{2,min}$ to increase, and eventually settle close to the actual efficiency η_2 . This will diminish overcharging of the ultra-capacitor with progress of time.

Voltage fluctuation is undesirable in power networks. Therefore, the aforementioned modulation method, even though is capable of inducing the fuel cell to improve its $\eta_{2,min}$ estimate, must be designed in a way such that voltage fluctuations are low and they diminish as the estimate of $\eta_{2,min}$ improves. We propose V_L to be modulated by K_2 using an integral action

$$V_L = V_{L,nom} + k_{i,v2} \int_0^t (V_{uc} - V_{uc,d}) dt, \quad (3.14)$$

where $V_{L,nom}$ is the nominal load voltage. When V_{uc} is sufficiently close to $V_{uc,d}$, the integrator resets V_L to $V_{L,nom}$. On the other hand, an integrator is used in K_1 which is similar to Eq.(3.14) to utilize the voltage deviations from $V_{L,nom}$ for efficiency estimation.

$$\eta_{2,min}(t) = \eta_{2,min}(0) + k_{i,v1} \int_0^t (V_L - V_{L,nom}) dt \quad (3.15)$$

Since $\eta_{2,min}(0)$ is a lower bound Simulation results are depicted in Fig.3.7. In the simulation, pulsed changes in power demand were applied every 200s. Parameter values were $k_{i,v1} = 0.0005$, $k_{i,v2} = 0.005$, $\eta_2 = \bar{\eta}_2 = 0.8$, and $V_{L,nom} = 24V$.

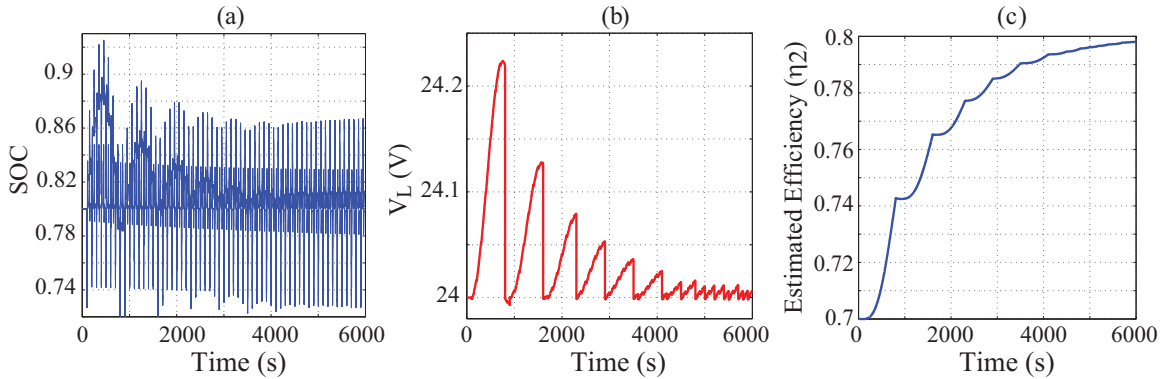


Figure 3.7: Simulations with Voltage Modulation and Efficiency Estimation

From Fig.3.7(a), it is clear K_2 is able to maintain the SOC through voltage modulation.

Further, Fig.3.7(b) shows that voltage fluctuations reduce over time. This is primarily due to better estimation of $\eta_{2,min}$ by K_1 over time. The estimation is depicted in Fig.3.7(c). The saw-tooth type of response as shown in Fig.3.7(b) is due to integrator resets. Another observation is that during higher SOC/voltage fluctuations toward the beginning, efficiency adaptation was faster, and it decreased with time. The estimation process therefore requires not only the voltage modulation but also requires persistent perturbations in the power demand.

CHAPTER 4: DETAILS OF PRACTICAL IMPLEMENTATION

4.1 Power Converter topologies

The power converters that were used for the construction of the hybrid power systems were essentially two-quadrant half-bridge converter, and as the name suggests, bidirectional power flow is allowed through the converter. The switches that were used are bidirectional in nature therefore they allow current flow both from drain to source and source to drain. The construction of the converter is shown in the fig. (4.1).

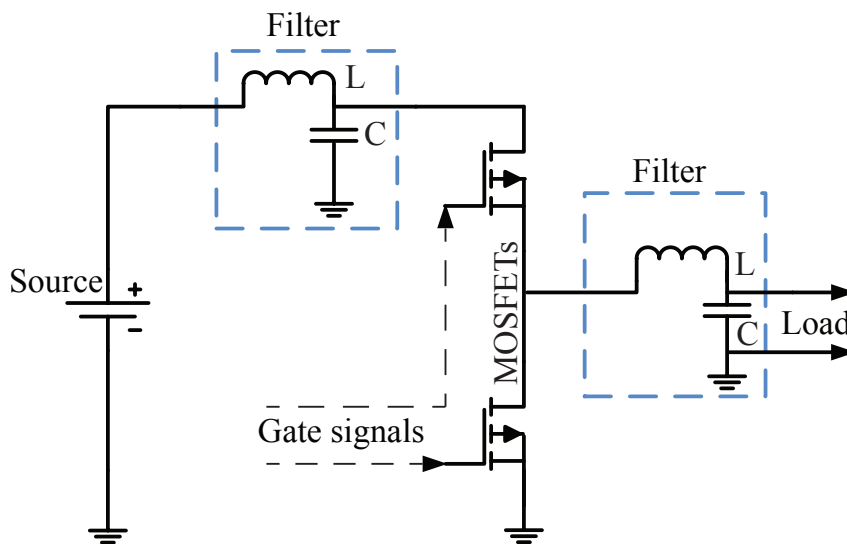


Figure 4.1: two-quadrant Power converter topology

However, according to standard cascaded PI control scheme, the bandwidth of the current compensator and voltage compensator are usually kept one order of magnitude higher/lower than the other one. For our case, provisions were made to switch between the voltage control

mode and current control mode. As discussed in the section 3, for the fuel cell network path a current regulate converter is required and for the ultra-capacitor path a voltage controlled power converter is needed. Therefore the respective converters were configured in the appropriate control mode as desired by the hybrid system. The internal architecture of the converters control circuit has been illustrated in figure 4.2. The settings of the value of the resistors and capacitors on the compensator circuit is tunable and usually used for achieving desired loop bandwidth of the respective control lops.

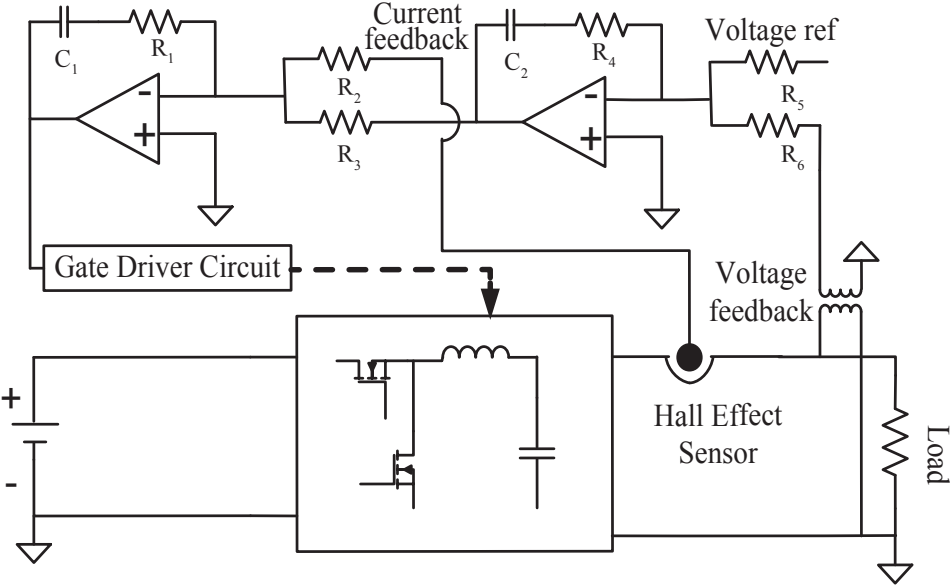


Figure 4.2: Power converter: Internal Control

As it is evident from the figure that there are 2 loops working at the same time. The voltage feedback from the load side voltage is fed to the compensator as the voltage feedback and a pre-set voltage reference is compared with that which generates the current reference for the current loop. Also a hall effect sensor is used to measure and subsequently feedback the load current value, which then again compared with the current reference generated by the

voltage loop and finally this determines the gate pulse width in the gate driver circuit block. Now, the resistance and capacitance sets of the each op-amp decides the cutoff frequency and bandwidth of each compensator. Therefore regulating these values $\{R_1, R_2, R_3, C_1\}$ and $\{R_4, R_5, R_6, C_2\}$ we can achieve a difference of atleast one order of magnitude difference in the bandwidth of each compensator in order for both the loops to work simultaneously. As shown in the fig.(4.2), both voltage and current feedback has been taken from the out put through voltage and current sensors respectively and fed back to the comparator embedded inside the converter to compare the desired and actual value of both the current and voltage. Therefore both the error signals were compensated through PI regulators.

However, in our application only single loop control appeared to be the requirement and provision has been made in the power converter so as to switch off any loop and use the other loop independently. In the event of this operation, any of the single loop, voltage or current when activated, will determine the required gate pulse width and generate according gate pulses. Therefore according to system requirements appropriate control loops were chosen and other loop has been put off.

4.2 Control of Unidirectional Converter C_1

As mentioned in section 3.1, and also evident from the development in sections 3.3, and 3.3.2.1, the DC/DC converter C_1 (see Fig.3.2) will be controlled in current control mode. To apply our theory directly, K_1 must command C_1 to deliver i_{fc} . However, referring to Fig.3.2, the converter C_1 in our setup allows us to command i_o directly and not i_{fc} . The DC-DC converter has an in-built controller which takes a sensed feedback of i_o flowing through a hall-effect sensor inside the converter, and using a PI-controller, makes i_o tend towards a commanded value $i_{o,c}$ set by the user. To control i_{fc} through C_1 , we propose the following

feed-forward and feedback combination:

$$i_o = i_{o,c} = \frac{\bar{\eta}_1 V_{fc} i_{fc,cal}}{V_L} + k_{p,1} e_{fc} + k_{i,1} \int_0^t e_{fc} dt, \quad e_{fc} \triangleq i_{fc,cal} - i_{fc} \quad (4.1)$$

where $\bar{\eta}_1$ is a constant estimated efficiency of C_1 , i_{fc} is the measured fuel cell current, and $i_{fc,cal}$ is the target fuel cell current calculated using Eqs.(3.6) and (3.7), as $i_{fc,cal} = 4nFU_{ss}\dot{N}_f/(\mathcal{N}_{cell}\beta)$. The internal controller in C_1 generates fast response, on the order of micro-seconds. Hence we assume $i_o = i_{o,c}$ in Eq.(4.1). The feed-forward term ($\bar{\eta}_1 V_{fc} i_{fc,cal}/V_L$) in Eq.(4.1) comes from the power balance at the input and output terminal of the converter C_1 . The sequence of signal flow is explained through the schematic in Fig.4.3.

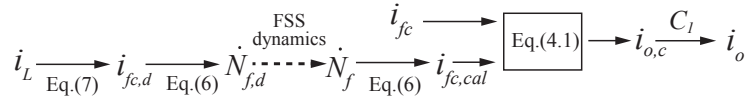


Figure 4.3: Schematic of Signal Flow in K_1

To prove that the above approach will lead to convergence of i_{fc} to $i_{fc,cal}$, we assume that the feed-forward term is constant during the correction interval, which is reasonable if $k_{p,1}$ and $k_{i,1}$ are assigned relatively high values. Referring to Fig.4.3 and Eq.(4.1), we then have

$$\frac{di_o}{dt} = \frac{\eta_1 V_{fc}}{V_L} \frac{di_{fc}}{dt} = k_{p,1} \dot{e}_{fc} + k_{i,1} e_{fc} \Rightarrow \left(k_{p,1} + \frac{\eta_1 V_{fc}}{V_L} \right) \dot{e}_{fc} + k_{i,1} e_{fc} = 0 \quad (4.2)$$

In conclusion, Eq.(4.2) guarantees that $\lim_{t \rightarrow \infty} e_{fc} \rightarrow 0$, provided the inequalities $k_{p,1} > -\frac{\eta_1 V_{fc}}{V_L}$ and $k_{i,1} > 0$ are satisfied.

4.3 Bidirectional Converter Control

The bidirectional converter C_2 is operated in voltage control mode. The primary purpose of this converter is to maintain a constant voltage across the load at all times. The converter has been set to maintain $V_L = 23V$ across the load for the dissipation based method. The choice of this value for V_L is driven by the limiting output voltage of C_2 , which is 23.3V.

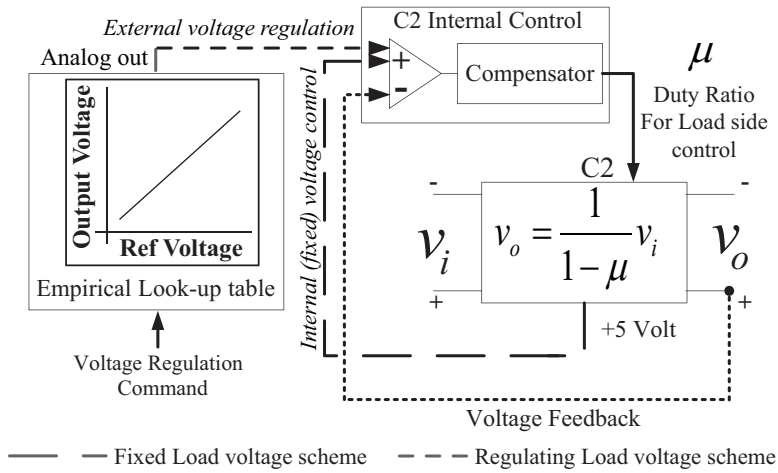


Figure 4.4: Implementation of External Voltage Modulation on C2

4.4 η_1 Measurement

In calculating $i_{fc,d}$ in Eq.(3.7), it is assumed that the measurement of η_1 is available to K_1 , since it is a local variable. In our experimental setup it is measured by implementing the power balance equation for C_1 to generate a coarse measurement $\eta_{1,m}$, followed by a first order filter of time constant τ for smoothing

$$\eta_{1,m} = \frac{V_L i_o}{V_{fc} i_{fc}}, \quad \dot{\bar{\eta}}_1 = (1/\tau) (\eta_{1,m} - \bar{\eta}_1) \quad (4.3)$$

4.5 PWM Switching Circuit

The approach that was taken in Chapter 3, in equation 3.12 was essentially to dissipate excess energy by varying the resistance or conductance of the dissipator. However, in practice we keep the resistance constant and change the average voltage appearing across it, therefore the same effect can be achieved here with a little modification in the theory proposed in chapter 3. Controller K_2 manipulates the duty ratio μ to change the dissipation rate as follows:

$$\mu(t) = \frac{k_{p,uc}}{V_{uc}}(V_{uc}-V_{uc,d}) + \frac{k_{i,uc}}{V_{uc}} \int_0^t (V_{uc}-V_{uc,d}) dt, \begin{cases} \dot{\mu} = 0, & \text{if } \mu = 1 \text{ and } V_{uc} > V_{uc,d} \\ \mu = \dot{\mu} = 0, & \text{if } V_{uc} \leq V_{uc,d} \end{cases}, \sigma_R = \mu\sigma_{R,max} \quad (4.4)$$

The average voltage appearing across the dissipating resistor, effectively determines the i_R . The relation between the duty ratio $\mu(t)$ and i_R can be formulated as:

$$\frac{1}{T} \int_0^T V_{uc} d_R(t) dt = i_R R \quad (4.5)$$

where $1/T$ is the switching frequency of the PWM. The PWM circuit will be switched off as soon as the equilibrium $V_{uc} = V_{uc,d}$ is established. The hardware consists of a simple solid-state switch which drives the gate of a power MOSFET of appropriate rating whenever the ultra-capacitor voltage surpasses a certain threshold voltage. The voltage reference is set to $12.2V$ above which the PWM circuit activates. Moreover, the rate of discharge is controlled by the pulse-width of the PWM signal that is realized by driving the gate of the MOSFET. The gate driver circuit consists of $UCC27322$ gate driver IC which can produce $9A$ peak current at the Miller Plateau region of the MOSFET [45]. Schematics and hardware of the PWM circuit are shown in Fig.4.5.

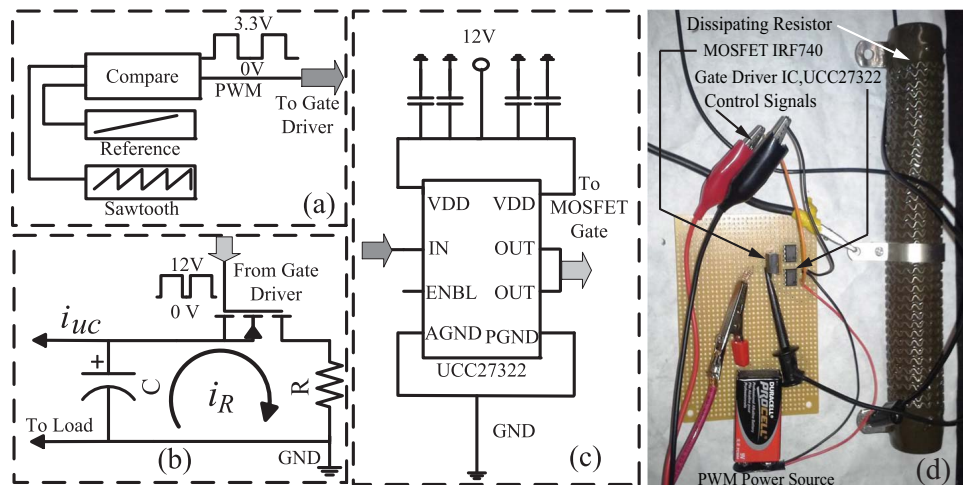


Figure 4.5: (a) Schematic for PWM generator. (b) Discharge Circuit. (c) Gate Driver. (d) Switching Circuit.

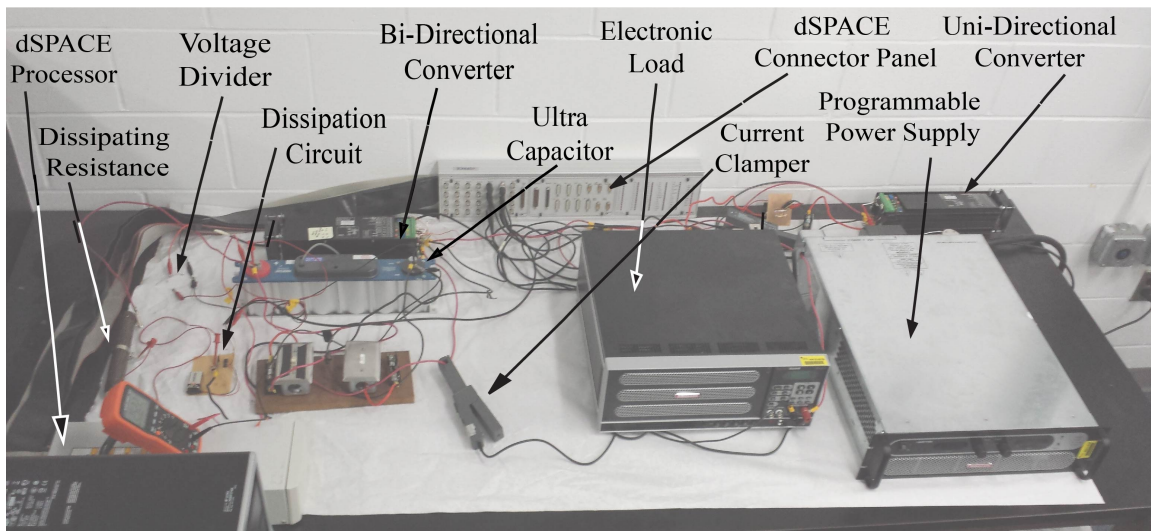


Figure 4.6: Experimental Test Stand

The hardware setup is illustrated in the fig.(4.6). The specifications of the equipment used here in the figure are tabulated in the table.(4.1).The hardware in the loop (HIL) approach

was implemented in the real time processor Dspace.

Table 4.1: Equipment specifications

Item	Specification(Voltage)	Specification(Current)	Other Specification	Make
dSpace	i/p:120V AC	-	-	dSpace1103
Power Supply	110V AC/DC	o/p:50A	Programmable	Ametek SGA100/50
Electronic Load	i/p:120V AC	0-120A, 0-1.8KW, 0-1790ohm	Programmable	Sorenson SLH
Ultracapacitor	16.2V DC	-	250F	Boostcap, BMOD0250 P16
Unidirectional Converter	44-50V DC	40A	Programmable	Zahn Elect. DC-5050F-SU
Bidirectional Converter	44-50V DC	40A	Programmable	Zahn Elect. DC-5050F-SU
Current Sensors	-	1-100A	Bandwidth 100KHz	Fluke-80i-110S
Voltage Sensors	0-1KV	10mA	Resistance divider	-

The mathematical model of the SOFC and its characteristics were embedded in the Dspace, and the response of the theoretical model was sent in real time to a programmable DC power supply given in table.4.1. Hence, the Dspace and the programmable DC power supply collectively represented the SOFC system, however limited by the accuracy of the theoretical model. Along with the HIL, both the controllers K_1 and K_2 mentioned in section.3.3.2.1 and section.3.3.2.2 and later on in section.3.3.3 were implemented in the Dspace processor. In addition to the implementation, another important function was served by the Dspace was to monitor the signals and values of different parameters of the system at all times, to ensure smooth operation of the system. The *Control panel* platform of the Dspace was used for all monitoring and parameter tuning in the middle of the operation. The figure below illustrates a typical control panel of Dspace platform during operation.

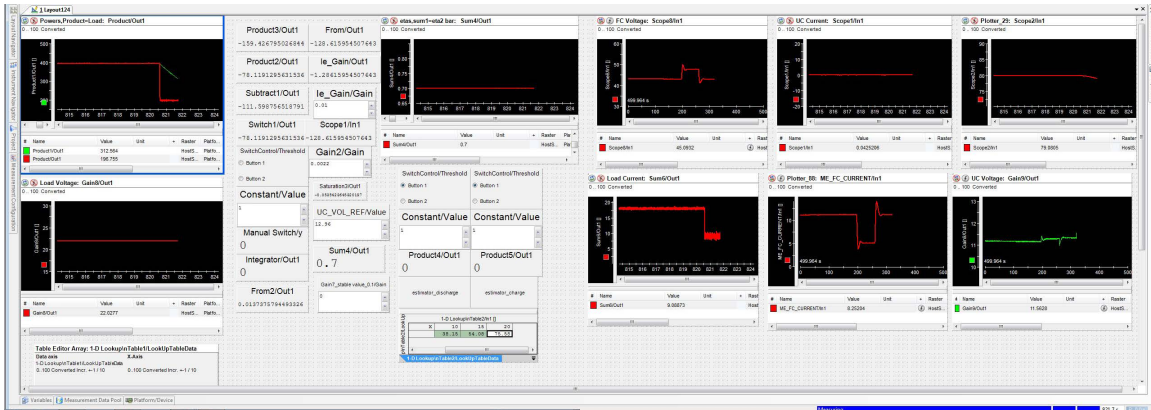


Figure 4.7: Typical Dspace control panel during operation

4.6 Experimental Results

The detailed experimental validation and the illustration of system behavior with a step load change has been demonstrated here in this section. Both dissipation and voltage regulation based approaches are discussed along with the experimental data obtained for both of them followed by a comparative study of the effect of both the approaches on system efficiency. The load resistance was given a periodic step change, usually from 1.2Ω to 2.4Ω , to test the system and controller response to a step change in the load and its performance, when this step change is persistent.

4.6.1 Experimental Validation of Dissipative Method

The decentralized approach with dissipation based SOC control, discussed in sections 3.3 and 3.3.2 is tested on the experimental setup and results are shown in Fig.4.8. As shown in Fig.4.8(a), a repetitive step load change from 10A level to 20A level is implemented. Fig.4.8(d) confirms transient fuel utilization control, with only $\approx \pm 2\%$ deviation about the

target $U_{ss} = 80\%$. Fig.4.8(b) and (e) are self-explanatory, representing fuel cell current and voltages. Fig.4.8(f) compares V_{uc} with (blue) and without (red) dissipation. For the test, we set $S_t = 0.75$, which corresponds to $V_{uc,d} \approx 12.2V$. The conservative nature of K_1 is clear, since it gradually overcharges the capacitor in the absence of dissipation (in K_2). With controlled dissipation the issue is addressed.

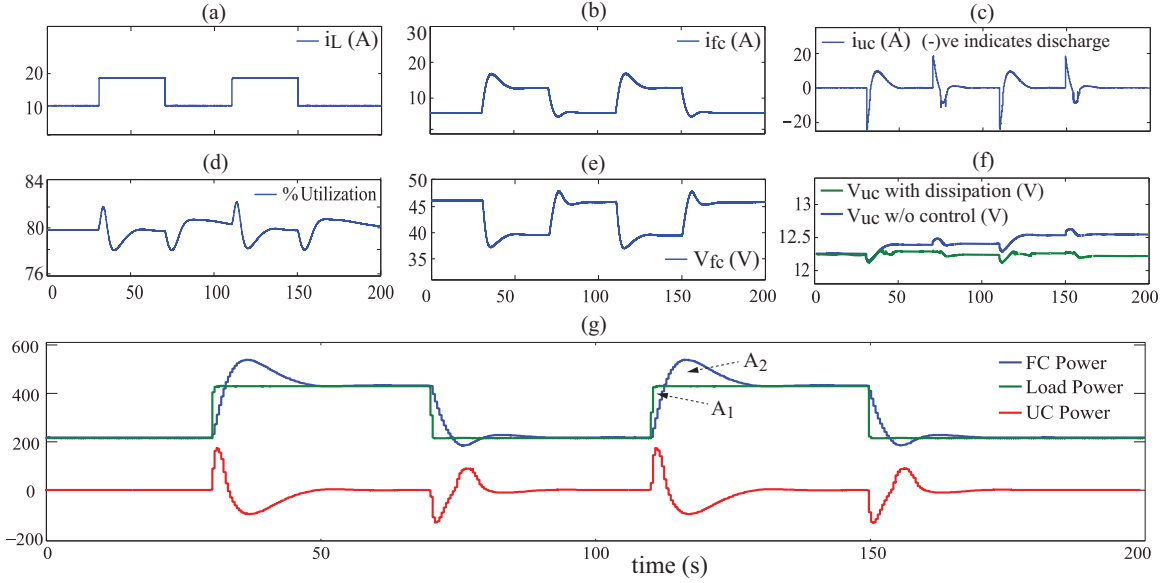


Figure 4.8: Experimental Results for Dissipation Based Approach

In the experiment, the controller parameters are chosen as follows: For K_1 , $k_i = 0.01$ in Eq.(3.7) and $k_{p,1} = k_{i,1} = 0.01$, $\bar{\eta}_1 = 0.85$, in Eq.(4.1) and for K_2 , $k_{p,uc} = 0$, $k_{i,uc} = 20$ in Eq.(4.4). In Fig.4.8(c), i_{uc} is plotted. As expected, i_{uc} goes to zero at steady-state, indicating that indeed the fuel cell supplies the entire power demand at steady-state. The slow response of the FC to the load changes, along with the capacitor's contribution to make up for FC's deficiency during load transients is visible in Fig.4.8(g). In this plot, also observe that $A_1 < A_2$. This is due to losses in C_2 which translates to Eq.(3.4) for conserving the capacitor's energy.

4.6.2 Experimental Validation of Voltage Modulation

Voltage modulation capability was facilitated in the converter C_2 with minor changes to its internal circuitry. Hardware limitations of C_2 limit the maximum $V_{L,nom}$ to $\approx 23.3V$. Hence, to allow voltage modulation $V_{L,nom} = 22V$ is chosen in Eq.(3.14). The modifications to C_2 to implement voltage modulation are shown in Fig.4.4.

Two integrators were used at the FC side (i.e. K_1) to utilize the load deviations from 22V for efficiency estimation, to account for the different discharging and charging efficiencies, namely η_2 and $\bar{\eta}_2$ respectively.

$$\begin{aligned} \hat{\eta}_2(t) &= \hat{\eta}_2(t_0) + k_{i,v11} \int_0^t (V_L - 22) dt, & \dot{\hat{\eta}}_2 &= 0, & \text{when discharging} \\ \hat{\bar{\eta}}_2(t) &= \hat{\bar{\eta}}_2(t_0) + k_{i,v12} \int_0^t (V_L - 22) dt, & \dot{\hat{\bar{\eta}}}_2 &= 0, & \text{when charging} \end{aligned} \quad (4.6)$$

In the experiment, the following parameter values were chosen, $k_{i,v2} = 0.1$, $k_{i,v11} = 0.001$, $k_{i,v12} = 0.002$ and $\hat{\eta}_2(t_0) = \hat{\bar{\eta}}_2(t_0) = 0.7$. The experimental results are shown in Fig.4.9.

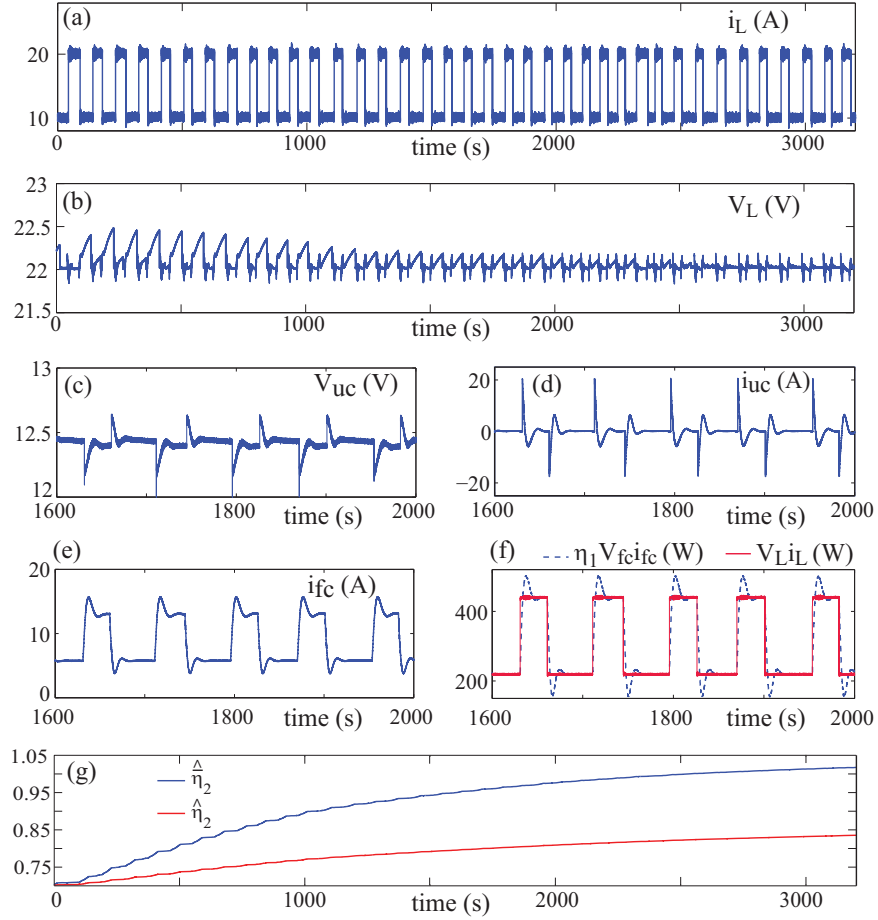


Figure 4.9: Experimental Results for Voltage Regulation Based Approach

The power draw was pulsed at regular interval, as shown in Fig.4.9(a). Figure 4.9(b) is the main result of the experiment, showing that load voltage fluctuations imposed by K_2 diminished over time starting from $\sim 0.5V$ to $< 0.05V$. This is because with progressive improvement of the efficiency estimates, the net capacitor overcharge over individual power pulses reduce. The corresponding variations in V_{uc} , i_{uc} and i_{fc} are depicted in Figs.4.9(c), (d) and (e) respectively. The load power and fuel cell delivered power are plotted in Fig.4.9(f). The figure illustrates how K_1 modulates the fuel cell power to attain energy conservation

in the ultra-capacitor. The estimates $\hat{\eta}_2$ and $\hat{\hat{\eta}}_2$ are shown in Fig.4.9(g). The estimates of discharge and charge efficiencies settle at $\hat{\eta}_2 \approx 0.84$ and $\hat{\hat{\eta}}_2 \approx 1.02$ respectively. This, in particular $\hat{\hat{\eta}}_2 \approx 1.02$ is expected since it represents the charge efficiency. As mentioned in section.3.1 and section.3.2, the charge efficiency is expected to be greater than 1 since the energy supplied for charging the ultracapacitor will be higher than the change in the stored energy due to losses.

4.7 System Loss Comparison

Although both the approaches described above performs satisfactorily on the task of meeting the control objectives described in section 3.2, they have certain advantages and disadvantages which makes each approach more applicable in different perspectives. The voltage regulation based approach progressively reduces energy losses; yet it relies on persistent excitation of the load to improve its efficiency estimates. On the other hand, the dissipation based approach results in uniform energy loss, but it does not require perturbations on the network. The energy losses with each approach were compared and plotted in Fig.4.10. Each data point represents an average power loss over an interval, calculated as

$$W_{loss,i} = \frac{1}{t_i - t_{i,0}} \int_{t_{i,0}}^{t_i} (V_L i_L - V_{fc} i_{fc}) dt \quad (4.7)$$

for both approaches. In Eq.(4.7), $\Delta t_i = t_i - t_{i,0}$ represents the i^{th} interval ending at t_i and starting at $t_{i,0}$. Each interval is roughly the same, around 100s, consisting of one step-up and one step-down in i_L . The final instants t_i were not all equally spaced in time. For example, $(t_5 - t_4)$ and $(t_7 - t_6)$ are longer than the others. It can be observed from the plot that with voltage regulation, the losses decay over time whereas it is uniform for the dissipation based approach. The overall magnitudes are not considerably different. This is because

the changes in capacitor voltage due to overcharging (and hence the required dissipation) were low in our experiments, owing to a high capacity of 250F and comparatively lower power levels, see Fig.4.8(f). It is expected that with lower capacity storage the advantages of voltage regulation will be more prominent.

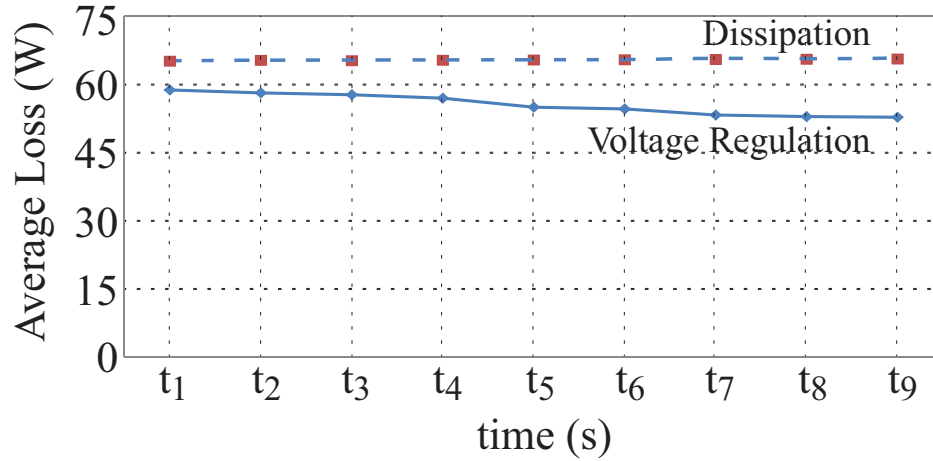


Figure 4.10: Power Loss patterns with Voltage Regulation and Dissipation based framework

However, although these verified data of the proposed decentralized scheme proves the effectiveness of the approach, it transpires that applicability of this approach to a highly scaled scenario is not a simple task. In fact, keeping this same approach and incorporating a large no of primary power sources in place of one single SOFC cell will make the decentralized design more challenging since all the estimation process described in section 3.3.3 are now required to be done separately for each of the sources and naturally that makes the problem highly complicated. Therefore, we needed a much simplistic and elegant approach to tackle more real life problem i.e microgrid. A concise description of the microgrid is given in the chapter-2. Moreover, in addition of more primary power sources, the load sharing between them in steady state is still not addressed with the present approach. For example, an equal load sharing between two SOFCs may be proposed on top of the existing framework, but

there is no provision has been made so that one SOFC will increase its production when the other SOFC is limited in production due to its internal constraints, in a decentralized manner. Therefore existing approach is apparently limited to small scale hybrid systems only. Therefore, there is a need for a much simpler control framework which employs the decentralized mode of operation and can be applied to large systems. Additionally, the new framework should be able to meet all the internal constraints posed by the controlled agents, i.e. power sources and also conforms to the power demand-supply condition. Following chapter will describe a newly proposed approach to effective deal with highly scaled version of the present problem.

4.8 Fault Tolerance Provisions in Decentralized Framework

As previously described in the section.1, an illustration of the fault tolerant attributes of the decentralized controller for the hybrid system is provided here. Referring to the previous works [41], the fuel cell current demand, $i_{fc,d}$ determines the fuel demand for the SOFC which is described by the following equation.

$$\dot{N}_{f,d} = \frac{i_{fc,d} \mathcal{N}_{cell}}{4nFU_{ss}} [1 - (1 - U_{ss})k] \quad (4.8)$$

where

$$i_{fc,d} = \frac{V_L i_L}{\bar{\eta}_1 V_{fc}} + g(E_s) + \delta_1 \quad (4.9)$$

where, $E_s = S - S_t$, S =SOC of the ultra capacitor and S_t = target SOC of the ultra capacitor. However in this paper, with a decentralized approach the demanded fuel cell current expression is as follows.

$$i_{fc,d} = \frac{V_L i_L}{\eta_1 V_{fc}} + k_i I_e, \quad k_i > 0 \quad (4.10)$$

Therefore it is clear from the above two equations that, in a centralized case, the SOFC controller depends on the value of the SOC of the ultra-capacitor whereas the decentralized controller is independent of the SOC. Therefore, in the event of a fault in the ultra-capacitor, its SOC will be perturbed. In a centralized control this will affect the SOFC fuel flow rate and possibly the fuel cell controllers will malfunction as well, whereas the decentralized controller, being invariant to the SOC of the ultra-capacitor, will ensure $\Delta P = V_L i_L - \eta_1 V_{fc} i_{fc}$, even under such a fault. However, depending upon the nature of the fault, for certain faults such as the one mentioned here, the advantage may be clear. But for others, a secondary protection may be necessary for both centralized and decentralized approaches.

CHAPTER 5: COUPLED DYNAMICAL SYSTEM APPROACH

Transitioning from the previous approach of decentralized control of multi DG microgrid systems, in this newly developed approach , we consider a large number of control nodes which represent each power sources. For a strategic load scheduling, we can incorporate loads in the set of control nodes as well. The external utility grid is also considered as a control node, however since the microgrid is much smaller and weaker than the utility grid, usually the external grid node is not controlled instead, it acts as an autonomous node. The load node is considered as the input node to the system, through which the load command is applied to the microgrid. The usual structure of a power network may often be simplified to a collection of local loads and a set of global loads which is supplied by all the power sources in the microgrid, which is represented by the load node L . The effect of local loads have been ignored as the main emphasis of this work, is to demonstrate decentralized control of multi DG system in a microgrid, therefore, the effective global load sharing among the power sources are sufficient to prove the effectiveness of the framework. The entire cyberphysical layer of the microgrid is mapped as a mathematical graph and all the analysis and design of the framework has been progressed from there.

The cyberphysical layer consists of the control and communication activities of a microgrid. This encompasses the control signal sent to each power source and the circuit protection elements in a microgrid, the communication topology between all the system elements and their interconnection, the processing of each signal from the measuring devices, the operators who decides the power sharing, the dynamic pricing, billing and all commercial activity, and so on. The framework that we want to achieve will significantly reduce the efforts in control room operations and manual tuning of power flow commands. The main objective of this framework is to control the transient active power flow and satisfy all the requirements of

smart operation of a microgrid as discussed before.

To simplify our analysis and design, we divide the operation of the cyberphysical layer into three distinct categories;

- Electricity Market, pricing, availability and economic dispatch calculation.
- Implementing dispatch commands through inverter controlled DGs.
- Measurements and estimations.

However, in conventional utility grid system, the economic dispatch calculations are done by distribution network operators (DNO) and it obtains a specific power output figure for each generator. In the following framework, these calculations of economic dispatch along with the local disturbances, system limitation(e.g. current, voltage, thermal limits etc) and manual override provisions are classified as the lower layer operation.

However, the market dependent load flow variations are slow process and our main objective in this work is to address the transient stability and transient load sharing problems as discussed in the chapters-1 and 2. The conventional droop control methods and other optimization based approaches have their own limitations. Therefore, we look for a novel decentralized approach in active power sharing among a large number of power sources connected to the microgrid and ensure smart operation. The decentralized approach is seen as the limited ability of a node or agent to interact with others. The dynamics of the controller itself has been defined as the upper layer operations. Therefore, in summary, any change in existing configuration of the load shares, any disturbance or manual intervention can be brought in through lower layer operation. While lower layer operation is non-functional, the upper layer and its current structure and configuration will dictate the share of loads among

the generators. This way a very flexible control structure can be realized which follows all the control objectives but when needed to be steered to a certain direction by users choice, there is no restriction to commit a manual steering operation.

5.1 System Description

The system structure under discussion is made into two different layers to separate out the functionality and hierarchy. The controller in the lower layer is primitive in nature and the main function is to monitor internal properties of the plant. If any distress call or manual command noted, it will communicate the safe operating value for the state to the upper layer. Whereas the upper layer solves more complex problem of distribution of the state values so that a certain constraint equation is met. The upper layer of control forms the basis of communication among the controllable nodes and determines the time response of the state for each of the node. In the fig.(5.1), the communication pattern in both the layers has been depicted. the proceedings of the discussion will assume highest amount of intra-node communication and later on effect of sparse communication will be examined.

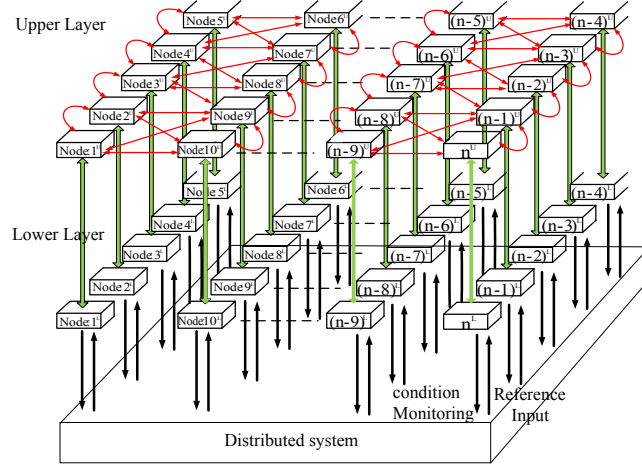


Figure 5.1: Two layer control structure

5.1.1 Model Development

We define here the controlling parameter/state of each node at the control layer as I_i , $i \in Z^+$, Z denotes set of integers, also n is the no of nodes. Also an exogenous input L with its state being represented as i_L which can be interpreted as power demanded by the load. Assuming a full connectivity among the nodes, i.e. each node is communicating with every other node in the upper layer of control, the interaction between the nodes can be modeled in a discrete equation as:

$$i_i(k\Delta t) = \sum_{j=1}^n a_{ij}i_j[(k-1)\Delta t] + b_i i_L[(k-1)\Delta t], \quad i = 1, 2, \dots, n \quad (5.1)$$

Which can be equivalently represented as a dynamical equation in continuous domain considering $\lim \Delta t \rightarrow 0$:

$$\dot{i}_i = \sum_{j=1}^n a_{ij}i_j + b_i i_L, \quad i = 1, 2, \dots, n \quad (5.2)$$

The communications are bidirectional everywhere hence, $a_{ij} = a_{ji}$. Physically, the interaction law states that each of the states will vary according to the state of the other nodes depending upon the topology of the communication. In the subsequent section we will examine the properties of the model and how they can be utilized to make a framework which will effectively control a set of distributed agents in a network. Therefore above equation can be written in the matrix form as;

$$\dot{I} = AI + BI_L \quad (5.3)$$

Where, $A = [a_{ij}]$ and $B = [b_i]$ and $A \in R^{n \times n}$ and $B \in R^n$. The parameter I or I_i , physically denotes the reference value of current/power, although in the paper it is frequently called state of a node, and \bar{I} denotes the steady state value of I .

5.1.2 Mapping On to a Graph

Like all the distributed control framework a mapping of the existing model on to an undirected Graph of appropriate edge and vertices will simplify analysis and further development. An undirected graph G has been defined as $G = (V, E)$ where vertices/nodes $V_j = \{v_1, v_2, \dots, v_n\}$ and edge $E_i = \{a_{11}, a_{12}, \dots, a_{21}, a_{22}, \dots, a_{31}, a_{32}, \dots, b_1, b_2, \dots\}$ where edge weights $a_{ij} \in R$. Therefore we have a real weighted edge graph with an adjacency matrix consisting of the elements of E . The edge weights among the control nodes are denoted as a_{ij} and the edge weights between the control nodes and the exogenous node is denoted as b_i . An equivalent pictorial representation of an arbitrary no of nodes of the graph is shown here. To keep a parity between the dynamical equation and the graph, we define the adjacency matrix as, $Q = \begin{bmatrix} A & B \\ B^T & 0 \end{bmatrix}$.

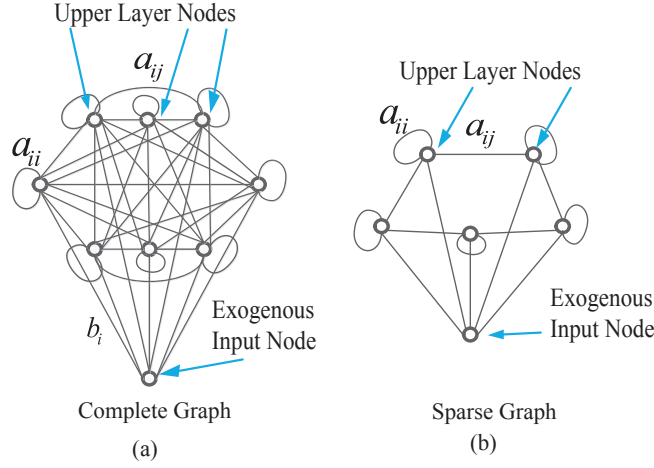


Figure 5.2: Mapped Graph

An assumption has been made here, that the graph is always a spanning tree, therefore each node will have a direct or indirect connectivity with every other node in the network.

5.2 Proposed Framework

In this section the proposed framework to control a set of distributed system with a decentralized scheme has been presented. The main objective of the control is to steer the set of distributed system to an equilibrium point which always satisfies a constraint equation. Here we define the possible set of equilibrium points as S , where $S = \{\bar{I}_i \in R, i \in Z^+ : \bar{I}_{i,max} \geq \bar{I}_i \geq \bar{I}_{i,min}\}$, however some practical limitation bounds S additionally. Throughout the discussion, S will be called the solution space. In the intended application area, the scenario can be interpreted as the load sharing problem in a power grid.

5.2.1 Problem Formulation

The decentralized control framework for a set of distributed system essentially requires only local sharing of the sensor information and local actuation of the control inputs. Therefore, the task here is to design a framework that work in decentralized fashion and realize the objectives listed below.

Objectives

- 1) The steady state constraint equation is required to be satisfied at all times, $\sum_{i=1}^n \bar{I}_i = I_L$, following a change in both \bar{I}_i and I_L .
- 2) The system is required to be controllable and stable.
- 3) The state distribution should adhere to its finite upper and lower limits, $\bar{I}_{i,max} \geq \bar{I}_i \geq \bar{I}_{i,min}$, $I_{i,min} \geq 0$.
- 4) Total implementation will be decentralized, i.e. all the nodes should only receive local data and control local actuation points, in other words, graph G should be weakly connected.

Assumptions

- 1) The lower layer controller monitors the state evolution and saturates it once any of the limits are reached.
- 2) The reference generated by the controllers are followed by the system/plant without any error.

- 3) At any point in time only one of the states is allowed to vary, for the sake of simplification in analysis.
- 4) The network graph is always a spanning tree.
- 5) The diagonal elements of A matrix, a_{ii} are user defined and chosen to be bigger than off diagonal element.

5.2.2 Reverse Cholesky Factorization

Note that the elements of A represent the coupling strengths between connected nodes. Referring to eqn.5.3, for stability of I , A must be Hurwitz. We will ensure this through a popular factorization method for any positive definite and symmetric matrix known as the Cholesky factorization [15]. Here the matrix A is represented as a product of a upper/lower triangular matrix and its transpose, whose diagonal elements are all positive. In this paper, a reverse approach has been adopted with some modifications to construct a negative definite matrix from a factor chosen a-priori in which all non-zero elements are real.

According to the decomposition form, the following lower/upper triangular matrix $\mathcal{L} \in R^{n \times n}$,

$$\mathcal{L} = \begin{bmatrix} \ell_{11} & 0 & 0 & \dots \\ \ell_{21} & \ell_{22} & 0 & \dots \\ \ell_{31} & \ell_{32} & \ell_{33} & \dots \\ \dots & \dots & \dots & \dots \end{bmatrix}, \ell_{ij} \in R \forall i \neq j, \text{ and } \ell_{ij} \in R^+ \forall i = j$$

will yield,

$$A = -\mathcal{L}\mathcal{L}^T = - \begin{bmatrix} \ell_{11}^2 & \ell_{11}\ell_{21} & \ell_{11}\ell_{31} & \dots \\ \ell_{11}\ell_{21} & \ell_{22}^2 + \ell_{21}^2 & \ell_{21}\ell_{31} + \ell_{22}\ell_{32} & \dots \\ \ell_{11}\ell_{31} & \ell_{21}\ell_{31} + \ell_{22}\ell_{32} & \ell_{31}^2 + \ell_{32}^2 + \ell_{33}^2 & \dots \\ \dots & \dots & \dots & \dots \end{bmatrix} \quad (5.4)$$

which is guaranteed to be a negative definite matrix for all entries of ℓ_{ij} , as long as they are real and the diagonal entries are real and positive. In this work, we utilize this Cholesky decomposition approach by first choosing the diagonal entries of A and then choosing the

off-diagonal entries ℓ_{ij} , $i \neq j$, and subsequently determining the diagonal entries of \mathcal{L} as follows, $\ell_{11} = \sqrt{A_{11}}$, $\ell_{22} = \sqrt{A_{22} - \ell_{21}}$, and so on. Therefore, the complete expression for the A matrix is,

$$a_{ij} = -\ell_{ij}\ell_{ii} - \sum_{\substack{k=1 \\ i \geq j}}^{i-1} \ell_{ik}\ell_{jk}$$

Hence from the given values of A_{ii} and arbitrarily chosen values for ℓ_{ij} one can construct a negative definite symmetric matrix A .

5.2.3 Steady State Solution and Constraint

In addition to A being Hurwitz, another important objective of this framework is to achieve steady state solutions under given constraints and being able to explore the permitted solution space S , as discussed at the beginning of section.5.2. The steady state solution of eqn.5.3, namely \bar{I} , can easily be found out by making $\dot{I} \rightarrow 0$,

$$\bar{I} = A^{-1}BI_L \tag{5.5}$$

The sign of I_L will be considered to be negative by convention, to signify a demand that is required to be met by all other nodes. Therefore we will use I_L here onwards as a negative quantity. We define a vector $C \in R^n$, where $C = [1 \ 1 \ 1 \ 1 \ \dots]$, so that from eqn.5.5, we can write,

$$C\bar{I} = CA^{-1}BI_L \tag{5.6}$$

Now from the objective, the constraint equation is $\sum_{i=1}^n \bar{I}_i = I_L$, which is equivalent to, $C\bar{I} = I_L$, therefore from eqn.5.6 we arrive at the steady state constraint equation,

$$CA^{-1}B = 1 \tag{5.7}$$

Now we define a vector $\Delta \in R^n$, where $\Delta = [\delta_1 \ \delta_2 \ \delta_3 \ \dots]^T$ so that, $\sum_{i=1}^n \delta_i = 1$ and $\delta_i \in R^+$, therefore $C\Delta = 1$. Substituting this in eqn.5.7, we get

$$A^{-1}B = \Delta \quad \Rightarrow \quad A\Delta = B \quad (5.8)$$

It also transpires that $\delta_i = \frac{I_i}{I}$, and $0 \leq \delta \leq 1$, physically which is the share of each state towards the constraint, or share of each generator towards the demand. Therefore the steady state eqn.(8) can be implemented to satisfy objective(1), listed section.5.2.1. We argue that given the designed structure of the network dynamics in eqn.5.3, the solution space of \bar{I} can be explored by only varying the elements of A matrix.

Remark: There exists a symmetric negative definite matrix $A \in R^{n \times n}$ and a vector $B \in R^n$, so that eqn.5.8 is always satisfied for an arbitrary $\Delta I_L \in S$. This result is obvious and can be concluded by looking at the expanded form of eqn.5.8 as the entries of B can be arbitrarily chosen without placing any restriction on the system dynamics.

5.3 Decentralized Implementation

So far the analysis has been done with a complete graph as the communication topology, however, reducing the number of edges will make the A matrix sparser and the amount of mutual communication reduces until it makes the topology completely localized with each vertices will only receive information about its one or two neighboring node depending on its position on the topology. As long as keeping the graph a spanning tree, the controllability aspect can be addressed [12],[14], however for the system given in eqn.5.3, some more detailed analysis on controllability and its dependence on the topology has been left for further research. Also the stability is being ensured all the time, only focus is due to be given to

the self-organization of the system under disturbances, which is the ability to hover around in the solution space keeping the steady state constraint satisfied due to disturbances in I_L or I_s . As pointed out in the previous section that any point on the solution space can be reached by only varying the a_{ij} entries, a simpler and elegant method is to be decided to tune up the a_{ij} parameters.

5.3.1 Linear Parameterization of a_{ij}

Since from the eqn.5.8, the number of unknowns in A is $\frac{n(n-1)}{2}$, which can be found out by simple series sum, and the number of equations are n , therefore as typically the distributed system contains more than one node, there will be infinite number of solutions for a_{ij} . Therefore a much simpler method is proposed here. The elements ℓ_{ij} is further parameterized in terms of δ_i as $\ell_{kj} = h_{kj}\delta_k$, $k \subset i$, where $h_{kj} \in R$. Therefore \mathcal{L} matrix becomes,

$$\mathcal{L} = \begin{bmatrix} \ell_{11} & 0 & 0 & \dots \\ h_{12}\delta_1 & \ell_{22} & 0 & \dots \\ h_{13}\delta_1 & \ell_{32} & \ell_{33} & \dots \\ \vdots & \vdots & \vdots & \dots \end{bmatrix}$$

where $\ell_{21} = h_{12}\delta_1$ and $\ell_{31} = h_{13}\delta_1$, for a varying δ_1 . Also to be noted, for a variation of δ_2 , ℓ_{21} is parameterized as $\ell_{21} = h_{21}\delta_2$. Similarly, each entry of \mathcal{L} matrix can be parameterized for any of the two possible δ_i variation, e.g. ℓ_{ij} can be parameterized for δ_i and δ_j variation and finally for a general variation in δ_k , the A matrix becomes,

$$A = -\mathcal{L}\mathcal{L}^T = - \begin{bmatrix} & & a_{1k} \\ & & a_{2k} \\ a_{k1} & a_{k2} & \vdots \\ & & \vdots \\ & & a_{nk} \end{bmatrix} \quad (5.9)$$

Essentially, corresponding row and column of A matrix except the diagonal elements, are multiplied by δ_i where i denotes the row and column number of A matrix. Now since each states are assumed to be varying one at a time, the symmetry of the A matrix is preserved

so is the negative definiteness in spite of all the variation in ℓ_{ij} due to parameterization, with $\ell_{ij} \in R$. since according to cholesky factorization in our case, any real positive value of off-diagonal ℓ_{ij} , A is negative definite.

Therefore, the entries of A matrix becomes a function of δ_i . $a_{ij} = -\ell_{ij}\ell_{ii} - \sum_{\substack{k=1 \\ i \geq j}}^{i-1} \ell_{ik}\ell_{jk}$ where $\ell_{kj} = h_{kj}\delta_k$, the elements of A becomes, $A = f(\delta_i)$ where $i \in Z^+$. Then the eqn.5.8 becomes a set of n unknowns in n no of equation and becomes solvable when implemented with any appropriate initial condition, and the problem is well posed.

Remark: An observation is made here that the construction of A according to eqn.5.4 and 5.9, essentially makes it a strictly diagonally dominant matrix [15], where *diagonal dominance* is defined as $\|a_{ii}\| \geq \sum_{\substack{i=1 \\ i \neq j}}^n \|a_{ij}\|$.

The approach of decentralized implementation has been illustrated in the fig.5.3. Here each node and its incident edges along with neighboring node is considered as a cluster. A cluster have all its internal information shared however there is no information shared between two clusters except the state of the overlapping nodes. Therefore with a weakly connected graph, the number of overlapping nodes are minimum and we can achieve a stable decentralized framework. Therefore, assuming a topology as per the fig.5.2(b), we can implement the cluster 1 constraint equation as follows,

$$\dot{I}_1 = a_{11}I_1 + a_{12}I_2 + a_{15}I_5 + b_1I_L \quad (5.10)$$

Similarly cluster 2 will be,

$$\dot{I}_2 = a_{12}I_1 + a_{22}I_2 + a_{23}I_3 + b_1I_L \quad (5.11)$$

Where b_1, b_2 etc can be implemented as per eqn.(8), i.e.

$$b_1 = a_{11}\delta_1 + a_{12}\delta_2 + a_{15}\delta_5 \quad (5.12)$$

and

$$b_2 = a_{12}\delta_1 + a_{22}\delta_2 + a_{13}\delta_3 \quad (5.13)$$

and so on. Each of the entry of Δ is then estimated as $\delta_i = \frac{I_i}{I_{L,c}}$, where $I_{L,c}$ is the calculated or actual value of the I_L which is obtained by summing all I_i s, and then the updated value of ℓ_{ij} is calculated based on the variation in δ_i as described in linear parameterization section. Hence the A matrix parameters can be obtained, which will be used in eqn.5.8 to generate updated values of the Δ parameters.

The implementation doesn't readily guarantees the objectives. Following proof will ensure, that the objective 1 is satisfied with this approach. We define an error tern $e = I_L + I_{L,c}$, therefore $\dot{e} = \dot{I}_{L,c}$ as I_L is constant. Hence $\dot{e} = \sum_{i=1}^n \dot{I}_i$.

Proposition: For the given system in eqn.5.3, with a implementation of A and B parameters as per eqn.5.4 and eqn.5.8 respectively with a parameterization described in eqn.5.9, the steady state constraint described in objective(1) will always be satisfied if A is diagonally dominant(see remark, section.5.3.1).

Proof: Considering eqn.5.3, applying the B vector parameters as per eqn.5.8 as decided before we get, $\dot{I} = AI + A\Delta I_L$, but again $I = \Delta I_{L,c}$, hence $\dot{I} = A\Delta(I_{L,c} + I_L)$. Therefore we can write, $\dot{e} = CA\Delta e$, where C is defined in section.5.2.3. Also, as per the reverse cholesky factorization, the $\ell_{ij} \in R^+$, therefore, it can be easily concluded that since A is assumed to be diagonally dominant and the diagonal components are negative after factorization by eqn.5.4, $s = CA = \sum_{i=1}^n a_{ij}$, is a row vector of entries all negative value, $s \in R^-$. therefore,

$s\Delta = \sum_{i=1}^n s_i \delta_i$. As discussed before, all δ_i are positive, so $CA\Delta < 0$. Hence we can conclude at steady state $\dot{e} \rightarrow 0$, which implies $e \rightarrow 0$, and the command I_L is restored by the rest of the states I_i , and objective 1 is satisfied. However, with a A matrix not being diagonally dominant, some interesting facts may arise. Also the inherent relation between the diagonal dominance and the negative/positive definiteness of A matrix is also an issue required to be investigated in future.

Even sparser topology would mean an attractive improvement of the economy of the design. So most sparse topology was tested which is detailed in the fig.5.6 where each nodes are connected to adjacent 2 nodes except the two terminal nodes and one of them is the exogenous input node, which are only connected to one adjacent node. The implementation has slightly been modified here without loosing the generality. The eqn.5.8 has been modified here as some of the nodes doesn't have information of I_L as, $AI = BI_L$. Naturally, for the nodes with no connectivity with node "L", the eqn.5.3 interprets as $\dot{I} = AI + \phi$, where $\phi \in 0^n$. Therefore the steady state value of these nodes remains unaltered in the event of a perturbation in I_L . Only nodes with connectivity to I_L , responds. Therefore, implementing the framework in a similar fashion as for the case of dense topology replacing δ_i with I_i , similar objectives can be met, and using lower layer control to balance out the state values a safe system operation can be conducted.

5.4 Stability

The stability of the given system can be assessed from a dynamical systems approach. From the eqn.5.3, the system is stable if the A matrix is negative definite. However, only that argument is not enough since point-wise stability does not guarantee stability of the system equilibrium since A matrix elements are changing with time according to the param-

eterization described in section.5.3.1. Therefore we will discuss the input-to-state stability subsequently.

The input-to-state stability of the system described in eqn.5.3 can be examined by choosing an appropriate Lyapunov function and following the analysis given in the appendix. Before going into the details of stability, for simplification let us assume, $Z = I - \bar{I}$, therefore from eqn.5.3, we can write, $\dot{Z} = \dot{I} = AZ + \bar{B}$ where $\bar{B} = (A\bar{I} + BI_L)$. Now from eqn.5.12,5.13, we note that the elements of B will be bounded as long as the A matrix elements are bounded. Also at steady state, the variable $\bar{B} \rightarrow [0]$. Therefore it is clear that \bar{B} has some bounds $\pm\mathcal{B}$ which is zero at steady state.

Proposition: The system in eqn.5.3 is input-to-state stable so long as matrix A is pointwise negative definite and symmetric.

Proof: We can convert the system in eqn.5.3 into standard form $\dot{Z} = f(t, Z, I_L)$, we define a lyapunov function $V = Z^T Z$, therefore, $\dot{V} = 2Z^T AZ + 2\bar{B}^T Z$. Assuming the maximum eigen value of A being λ_{max} , we can write, $\dot{V} \leq 2\lambda_{max}\|Z\|^2 + 2\mathcal{B}\|Z\|$. Simplifying, we have, $\dot{V} \leq 2\lambda_{max}(1 - \theta)\|Z\|^2$ for $\|Z\| > \frac{\mathcal{B}}{\theta|\lambda_{max}|}$, where $0 < \theta < 1$. Therefore if and only if A is negative definite and symmetric, λ_{max} becomes negative and $\dot{V} \leq 0$ for $\|Z\| < \frac{\mathcal{B}}{\theta|\lambda_{max}|}$. Hence we can conclude that for a bounded input I_L , the system is input-to-state stable (ISS) and the states are bounded. Furthermore, since \bar{B} goes to zero at steady state, hence at steady state, $\mathcal{B} \rightarrow 0 \implies \|Z\| \rightarrow 0$.

5.5 Structural Controllability

A detailed examination of the controllability of the pair (A, B) given in eqn.5.3 reveals whether a control input can drive the state of the system to a desired value. However, from

a physical aspect, analyzing structural controllability of the system will reveal the topological variance and its effect on the controllability of the system as shown in [38].

The control system given in eqn.(5.3), can be rewritten to bring it into a standard state space form $\dot{x} = Ax + Bu$, where $x = [x_1 x_2 x_3 \dots x_n]^T$. Considering in the grid connected mode the control variable being u and in the islanded mode the control variable being x_k where $k \subset i$, we can write the state space form as,

$$\dot{I}_i = \hat{A}I_j + \hat{B}I_k \quad j = 1, 2, \dots, k-1, k+1, \dots, i \quad (5.14)$$

$$\dot{I}_i = \hat{A}I_j + \hat{B}u \quad j = 1, 2, \dots, k, \dots, i \quad (5.15)$$

Proposition :The pair (A, B) is structurally controllable, if any of the following is true,

- 1) There is no permutation of coordinates, bringing the pair to one of the forms, $A =$

$$\begin{bmatrix} A_{11} & 0 \\ A_{12} & A_{22} \end{bmatrix},$$

$$B = \begin{bmatrix} 0 \\ b_2 \end{bmatrix} \text{ or } (AB) = \begin{bmatrix} P_1 \\ P_2 \end{bmatrix}.$$

- 2) The graph of (A, B) contains no nonaccessible node and no dilation.

- 3) The graph of (A, B) is spanned by a cactus¹.

Also, all of these conditions are mutually equivalent to each other.

A concise proof for the proposition has been presented in [38]. We will develop some further extension of the proofs to show that the system under consideration is structurally controllable depending on the topology variation in a weakly connected undirected graph.

¹Cactus is a connected graph in which any two simple cycles have at most one vertex in common[40].

Lemma 1: Every node of the complete graph of the system of eqn.(5.3) is accessible so long as G is a spanning tree.

Proof: Considering any vertex v_k , $k \in \{1, 2, 3, \dots, n\}$, the accessible vertex from v_k is denoted by T_1 , where $T_k = \{v_{k-1}, v_{k+1}\}$, similarly we can write for, vertex v_{k+1} or v_{k-1} , T_{k+1} and T_{k-1} . Now the accessibility of any vertex from another vertex can be defined by arguing that, if a one can reach the destination vertex starting from the origin traveling only in the direction of the edge [38]. Since, this is an undirected graph and a spanning tree, we can extend the set of accessible nodes for v_k , as $T_k = T_{k-1} \cup T_{k+1}$, and eventually, $T_k = T_{k-1} \cup T_{k+1} \cup \dots \cup T_{m-1} \cup \dots$, where $T_{m-1} = \{v_{m-2}, v_m\}$, hence with a spanning tree one can reach from any vertex to any other vertex in the set V_j , therefore with a spanning tree all vertex are accessible.

Lemma 2: The complete graph of the system of eqn.(5.3) is dilation free.

Proof: Considering a set S_1 formed by the vertices of the graph G , $S_1 = \{v_1, v_2, v_3, \dots, v_{n-1}\}$ excluding the origin or the exogenous node which is assumed to be v_n . Determining a set S_2 which contains all the nodes of V_j which has an edge from V_j to any node of S_1 . Therefore, for a complete graph, $S_2 = \{v_1, v_2, \dots, v_n\}$, as the graph is a spanning tree. Therefore $S_1 \subseteq S_2$, or the graph G is dilation free. Furthermore, a corollary to the previous proofs can be made;

Corrolary 1: Since the system is structurally controllable, therefore the graph is spanned by a cactus, according to the third proposition [38] and its equivalency to the structural controllability.

Therefore, without going into the technical details of a cactus graph, we can safely conclude from the two

Lemmas provided earlier, that as long as the communication topology of the controlling nodes are a spanning tree it shall remain controllable, which enables user to reduce number

of edges without harming the controllability of the system which justifies the assumption made in section.(5.2.1).

5.6 Lower Layer Operations

The lower layer usually command the state value when it is near saturation or during emergency situations, however proper design care has been taken so that no conflicting issue arises. The upper layer in usual time commands the plant where the lower layer observes the maximum possible limit for the state at that time, the command from upper layer is denoted as δ_i^u , and the observed maximum state value is denoted as δ_i^l and $\delta_{i,ref}$ is the actual reference command to the plant. Now the logic for switching of control authority between the lower and upper layer has been described by the following equation,

$$\delta_{i,ref} = \frac{1}{2}[(\delta_i^u + \delta_i^l) + (\delta_i^u - \delta_i^l)sgn(\delta_i^l - \delta_i^u)] \quad (5.16)$$

Also the δ_i^u is continuously updated to the actual $\delta_{i,ref}$ which drives the plant. In this way the two layers collaborates to drive the distributed plant/system. Fig.5.3 depicts the algorithm along with the upper layer control interaction.

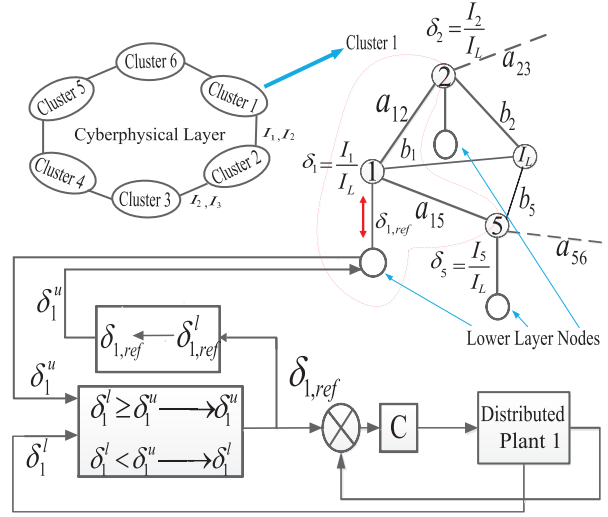


Figure 5.3: Decentralized Framework

The lower layer essentially takes care of the objective(3) and limits the states within certain bound $I_{i,max}$ and $I_{i,min}$.

5.7 Simulation and Results

The performance of the framework discussed so far, has been evaluated using Matlab Simulink environment. The variables of the design has been initialized to a known value so that all of the states reach some equal steady state values after closing the loop. Thereafter the lower layer control handle has been used to drive each of the state to a desired value and corresponding changes in the other states has been observed. The simulation has been initialized with a known and desired value of the δ_i s for topology 1, fig.5.4 and set of known I_i s for topology 2, fig.5.5.

A set of perturbations has been applied to the system, the sequence of which is, $I_L \rightarrow 2I_L$,

$I_5 \rightarrow \frac{I_5}{2}$ and $I_2 \rightarrow \frac{I_2}{2}$. A lower and upper limit has been set for each state, which is controlled by the corresponding lower layer. Therefore, $I_{1,max}$, $I_{3,max}$ and $I_{4,max}$ may approach close to the saturation values after the previous operation. Thus the maximum allowable deviation in state values is limited by the system limits.

A plot of all 5 states showing the response is given here along with the variation in graph weights. Also, since the a_{ii} 's were assumed to be given, this imposes a constraint on the implementation of the Reverse cholesky factorization approach. Since we are assuming only real elements for the A matrix, that prevents the elements of ℓ matrix to go beyond certain value in the process of self organization. From eqn.5.4 we can deduce a general form for the diagonal element of A with respect to the elements of ℓ as, $a_{ii} = \sum_{k=1}^{i-1} \ell_{ki}^2$. Hence, ℓ_{ki} is bounded by $\|a_{ii}\|$. Therefore, the choice of a_{ii} s will influence the system performance as well as the controllability, also this was left for further research and the current selection of a_{ii} s were made on a trial and error basis.

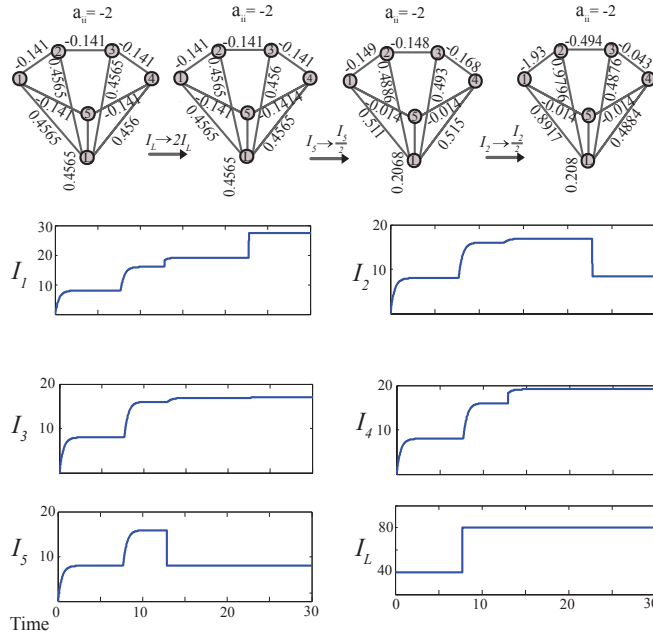


Figure 5.4: Simulation Result for topology 1

Also, the sparsest possible network has been examined as described in the previous section, while the difference in the topology produced different results but effectively the time to reach steady state was actually varied.

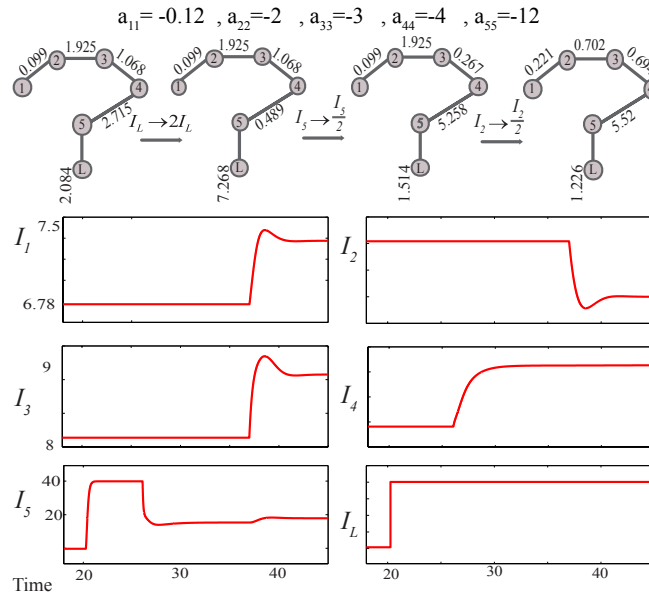


Figure 5.5: Simulation Result for topology 2

From the eqn.5.10 and 5.11, it is easy to conclude that if any node is not directly connected to some other node, the effect of the variation of the former on will reach the later through other path of the graph, and hence the weights in the substitute route will alter the transient response time as seen in the fig.5.6 where, the transient duration for a sparse graph and the same graph with an added edge has been plotted and it is visibly faster in case of a graph with more edges.

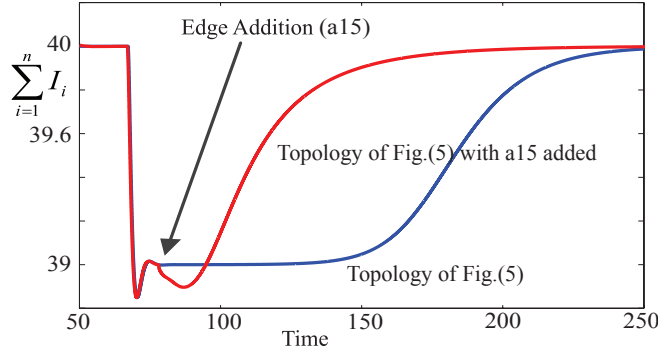


Figure 5.6: Effect of varying topology

For the topology 2, since the structure is significantly changed, the diagonal elements of A matrix had to be adjusted to get a feasible \mathcal{L} matrix as the restriction posed by the cholesky factorization mentioned before. The edge weights and their variation with each of the perturbations were recorded and presented here to have an understanding of their effect on the system evolution. Observing the simulation results, a number of important remarks can be made which explains the internal architecture of the control framework and the working procedure of the controller. As discussed before, the value of diagonal elements of the matrix A , a_{ii} s, are higher compared to the off diagonal element. This fact influences the steady state value each δ_i reaches after each step change occurs at one of the nodes. Therefore the solution of the eqn.(5.2), will be heavily dependent upon the diagonal entries of matrix A . Also, since the entries of A , a_{ij} are functions of the states I_i or I_j and the states are time varying in nature, therefore the eqn.(5.2) is linear time varying equation, which is thus solvable numerically. Therefore, a visual inspection of expanded discrete form of eqn.(5.2), which is eqn.(5.1) reveals that the steady state value, each of the state (I_i or δ_i) reaches after a step change in any of the nodes is approximately the sum of state

value before the change and a proportional component of the change. The proportionality is directly dependent on the corresponding $\frac{a_{ii}}{\text{trace}(A)}$ or $\frac{a_{ii}}{\sum_{j=1}^n a_{jj}}$. This analysis helps us comment on the approximate state values after each step change which keeps the framework predictable according to the design logic and the simulation results shown here confirms the analysis.

5.8 Overall Implementation In Power System

So far, we have developed a control framework that enables smart operation of a microgrid during the transient active power sharing between large group of power sources distributed. However, integrating this novel control framework with the power layer components such as inverters, transmission line, feeders and the utility grid is also an essential task to complete the endeavor to develop efficient microgrid systems. In chapter 2, a detailed description of existing control framework and their integration with power system layer has been described in brief. We will attempt to conceptually integrate the newly developed control framework with the power system layer of the grid.

Referring to the works [1, 2, 3], the power management block can be replaced with the coupled dynamical system framework developed in this chapter, which essentially replaces the power management calculations done by a conventional droop approach, and rest of the system may remain same. This essentially calculates the reference values for the voltage and speed set points for the inverters in the fig.(5.7).

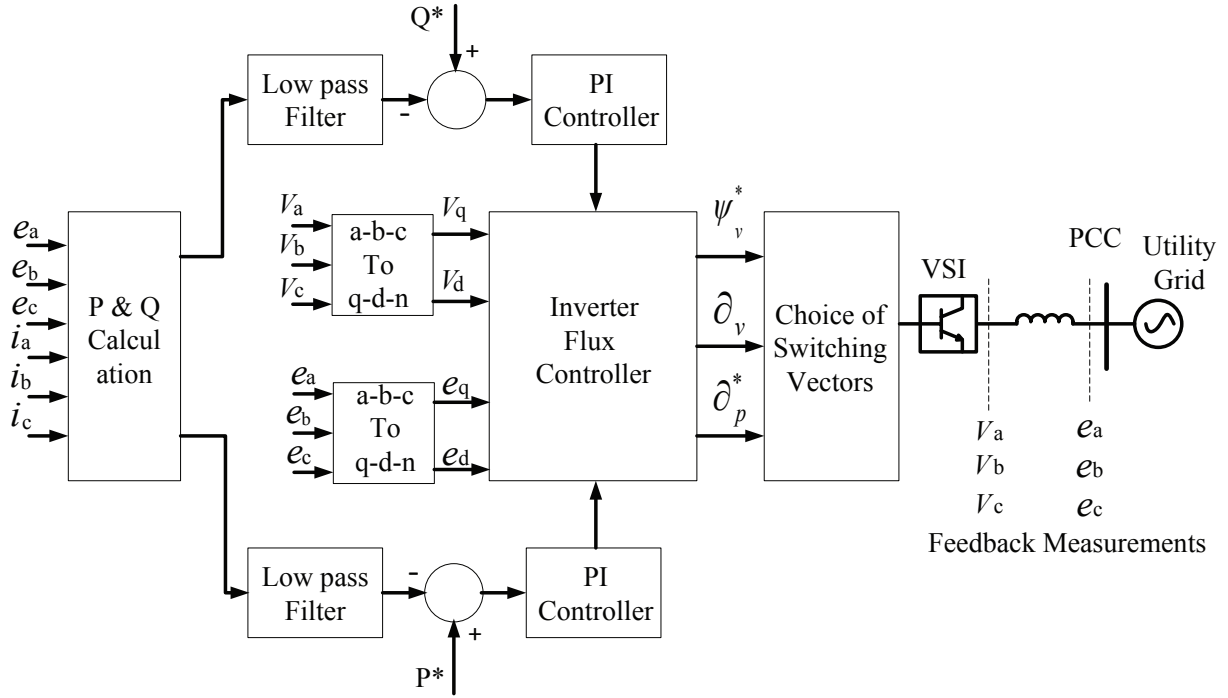


Figure 5.7: Inverter Control Scheme

The reference value for the active and reactive power here has been defined as P^* and Q^* respectively. Whereas the inverter terminal voltage vectors are denoted as V_a, V_b, V_c and the voltage vectors at the PCC is denoted as e_a, e_b, e_c . The hysteresis controller shown in the figure, controls both the active and reactive powers, P and Q respectively, to precisely follow the set points specified by P^* and Q^* . This forms the power system layer of the microgrid. Thus from the discussions in the section 5.1, the upper and lower layer control structure generates a reference value for the set point of the active power, for each power sources. hence, for n^{th} node of the network the share of active power is denoted as δ_n , which acts as the reference for the active power generation P_n^* . The switching vector selection is done using space vector pulse width modulation technique(SVPWM). For the works in [1, 2],

the inverter flux control has been done using a hysteresis controller and the appropriated switching vector selection tables and analysis has been given in [63]. A similar approach is taken for the implementation of the power system layer here in this work. Therefore, putting all the layers together we get a complete picture of the microgrid. The lower layer is used to manually tune or set the out put of any source as desired by the user, the upper layer coordinated among all the power sources and distributed the load among all the sources according to the current configuration of the graph edge weights and the power system layer takes the reference values generated by the two layer control system and implements them so that the load distribution follows the references. A pictorial representation of the overall system is shown in the following figure.

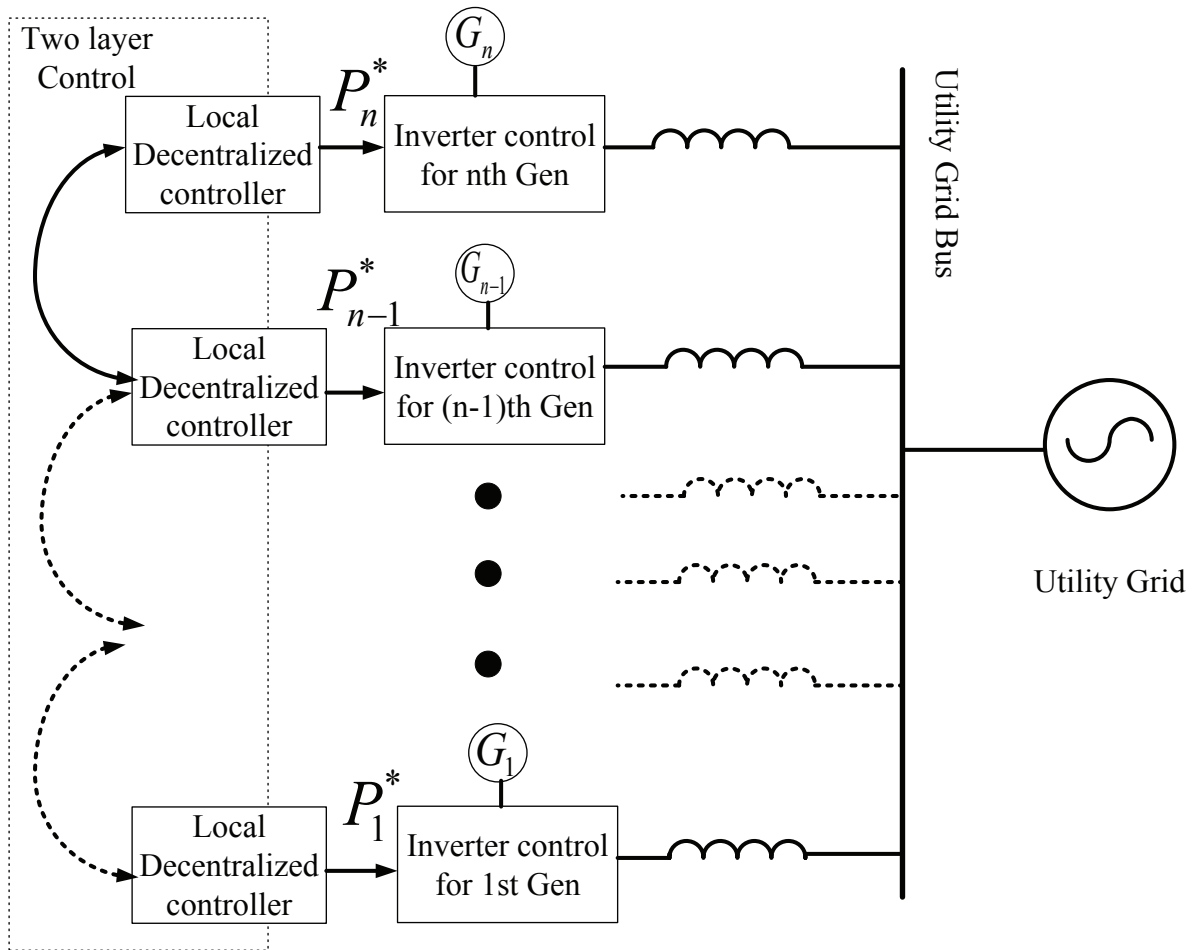


Figure 5.8: Overall system diagram Combining power system layer and control layer

Therefore the proposed control framework demonstrates the ability to operate a microgrid with performance specifications mentioned in the beginning of this chapter, while successfully supplying the demanded load.

CHAPTER 6: CONCLUSION

The impact of the decentralized control on power grid are getting more important every day. Considering the vision of a smart grid, the ability to plug-and-play, network flexibility, outage management as well as the source/load side power management being the most important aspects, a decentralized framework is becoming an absolute necessity as it enables all of the aforementioned attributes in a microgrid. The discussion so far addressed a small scale design of a hybrid power system consisting of a SOFC and an ultra-capacitor. From that discussion, a scaled up version of the problem, i.e for a large microgrid having a large number of sources interconnected, the load sharing problem is addressed in a decentralized manner using coupled autonomous systems approach, without using the expensive leader based controller and only with local information sharing between nodes. The stability which is a key issue with any control design was addressed in sufficient detail for both the cases. For SOFC ultra-capacitor hybrid system, with conventional stability approaches of a differential equation and for the coupled dynamical system approach, using reverse Cholesky factorization method elaborated in section.5.2.2. The ability of the framework to move from one equilibrium point to another without sacrificing performance was also demonstrated in section.5.7. The system parameters and their effect on the performance are one fairly explored issue however it is obvious that with the increase in the complexity of the topology, a wide band of interesting phenomenon might appear to the surface. Some of those possibilities were noted in respective sections of the paper. A different coupling method other than that is demonstrated in this work might bring in some interesting outcome to the solution of this problem. As a whole, the framework satisfies all its objectives, with promises of flexibility, reliability and resilience.

APPENDIX : INPUT TO STATE STABILITY

According to [13], any system defined by $\dot{I} = f(t, I, I_L)$, is said to be input-to-state stable (ISS) if there exists a class \mathcal{KL} function β and a class \mathcal{K} function γ such that for any initial state $I(t_0)$ and any bounded input $I_L(t)$, the solution $I(t)$ exists for all $t \geq t_0$ and satisfies $\|I(t)\| \geq \beta(\|I(t_0)\|, t - t_0) + \gamma(\sup_{t_0 \leq \tau \leq t} \|I_L(\tau)\|)$. A Lyapunov approach to investigating ISS is;

Theorem: Let $V : [0, \infty] \times R^n \rightarrow R$ be a continuously differentiable function such that

$$\alpha_1(\|I\|) \leq V(t, I) \leq \alpha_2(\|I\|) \quad (.1)$$

$$\frac{\delta V}{\delta t} + \frac{\delta V}{\delta I} f(t, I, I_L) \leq -W_3(I), \quad \forall \|I\| \geq \rho(\|I_L\|) > 0, \quad (.2)$$

$\forall (t, I, I_L) \in [0, \infty] \times R^n \times R^m$, where α_1 and α_2 are class \mathcal{K}_∞ functions, ρ is a class \mathcal{K} functions and $W_3(I)$ is a continuous positive definite function on R^n . Then the system $\dot{I} = f(t, I, I_L)$ is input-to-state stable.

LIST OF REFERENCES

- [1] Katiraei, F.; Iravani, M.R., "Power Management Strategies for a Microgrid With Multiple Distributed Generation Units," *Power Systems, IEEE Transactions on* , vol.21, no.4, pp.1821,1831, Nov. 2006.
- [2] Chandorkar, M.C.; Divan, D.M.; Adapa, R., "Control of parallel connected inverters in standalone AC supply systems," *Industry Applications, IEEE Transactions on* , vol.29, no.1, pp.136,143, Jan/Feb 1993.
- [3] Katiraei,F.; Iravani,M. R.; and Lehn,P. W., "Micro-grid autonomous operation during and subsequent to islanding process," *IEEE Trans. Power Del.*, vol. 20, no. 1, pp. 248?257, Jan. 2005.
- [4] Tuladhar, A.; Jin,H.; Unger,T. and Mauch,K., "Operation of single phase inverter modules with no control interconnections," in *Proc. IEEE APEC,1997*, pp. 94-100.
- [5] Majumder, R.; Ghosh, A.; Ledwich, G.; Zare, F., "Control of parallel converters for load sharing with seamless transfer between grid connected and islanded modes," *Power and Energy Society General Meeting - Conversion and Delivery of Electrical Energy in the 21st Century, 2008 IEEE* , vol., no., pp.1,7, 20-24 July 2008.
- [6] Marwali,M. N.; Jung,J.W. and Keyhani,A., "Control of distributed generation systems",Part II: Load sharing control," *IEEE Trans. Power Electron.*, vol. 19, no. 6, pp. 1551?1561, Nov. 2004.
- [7] Chen, C.; Nagananda, K.G.; Gang, X.; Kishore, S.; Snyder, L.V., "A Communication-Based Appliance Scheduling Scheme for Consumer-Premise Energy Management Systems," *Smart Grid, IEEE Transactions on* , vol.4, no.1, pp.56,65, March 2013.

- [8] Seon-Ju, A.; Soon-Ryul, N.; Joon-Ho, C.; Seung-Il, M., "Power Scheduling of Distributed Generators for Economic and Stable Operation of a Microgrid," Smart Grid, IEEE Transactions on , vol.4, no.1, pp.398,405, March 2013.
- [9] Carvalho, P.M.S.; Correia, P.F.; Ferreira, L.A.F.M., "Distributed reactive power generation control for voltage rise mitigation in distribution networks," IEEE Trans. Power Syst. 23, 766-772 (2008)
- [10] Zhang,H.; Lewis,F.L. and Das,A., "Optimal design for synchronization of cooperative systems: state feedback, observer and output feedback," IEEE Trans. Automatic Control, vol. 56, no. 8, pp. 1948-1952, August 2011.
- [11] Maknouninejad,A.; Lin,W.; Harno,H.G.; Qu,Z.; and Simaan,M.A. "Cooperative Control for Self-Organizing Microgrids and Game Strategies for Optimal Dispatch of Distributed Renewable Generations," Springer's Journal of Energy Systems, vol.3, no.1, pp.23-60, 2012.
- [12] Olfati-Saber,R.; Fax,J. and Murray,R., Consensus and cooperation in networked multi-agent systems, Proc. IEEE, vol. 95, no. 1, pp. 215-233, Jan. 2007.
- [13] Khalil, H.K., Nonlinear Systems, 3rd edn. Prentice-Hall, Upper Saddle River (2002).
- [14] Ching-Tai, L., "Structural controllability," Automatic Control, IEEE Transactions on , vol.19, no.3, pp.201,208, Jun 1974
- [15] Meyer, Carl.D. Matrix Analysis and Applied Linear Algebra, SIAM.
- [16] Smallwood, C. L., "Distributed generation in autonomous and non-autonomous micro grids," inProc. IEEE Rural Electric Power Conf., May 2002, pp. D1/1D1/6.
- [17] Lasseter, R. H. and Piagi, P., "Microgrid: A conceptual solution," in Proc. Power Electronics specialists Conf., Aachen, Germany, Jun. 2004, vol. 6, pp. 4285-4290.

- [18] Milanovic, J. V. and David, T. M., "Stability of distributed networks with embedded generators and induction motors," in Proc. IEEE Power Eng. Soc. Winter Meeting, New York, Jan. 2002, vol. 2, pp. 10231028.
- [19] Katiraei, F.; Iravani, M. R.; and Lehn, P. W., "Small-signal dynamic model of a micro-grid including conventional and electronically-interfaced distributed resources," Proc. Inst. Elect. Eng., Gen., Transm. Distrib.
- [20] Coelho, E. A. A.; Cortizo, P. C.; and Garcia, P. F. D., "Small-signal stability for parallel-connected inverters in stand-alone AC supply systems," IEEE Trans. Ind. Appl., vol. 38, no. 2, pp. 533542, Mar./Apr.2002.
- [21] Ming. H; Haibing. H; Yan. X; Guerrero, J.M., "Multilayer Control for Inverters in Parallel Operation Without Intercommunications," Power Electronics, IEEE Transactions on , vol.27, no.8, pp.3651,3663, Aug. 2012
- [22] Xin, H.; Qu, Z.; Seuss, J.; Maknouninejad, A., A Self-Organizing Strategy for Power Flow Control of Photovoltaic Generators in a Distribution Network.
- [23] De Brabandere, K.; Bolsens, Bruno; Van den Keybus, J.; Woyte, A; Driesen, J.; Belmans, R., "A Voltage and Frequency Droop Control Method for Parallel Inverters," Power Electronics, IEEE Transactions on , vol.22, no.4, pp.1107,1115, July 2007.
- [24] Majumder, R.; Ghosh, A; Ledwich, G.; Zare, F., "Power System Stability and Load Sharing in Distributed Generation," Power System Technology and IEEE Power India Conference, 2008. POWERCON 2008. Joint International Conference on , vol., no., pp.1,6, 12-15 Oct. 2008.
- [25] Mohan, N.; Undeland, T. M.; Robbins, W. P., "Power Electronics: Converters, Applications, and Design", Wiley, 1989.

- [26] Sinden, G., "Assessing the Costs of Intermittent Power Generation", UK Energy Research Centre, 5 July 2005.
- [27] Kuntz, M. T.; Dawe, J. , "renewable. rechargeable. remarkable.". VRB Power Systems. Mechanical Engineering. Retrieved 2008-10-20.
- [28] Samantha, .; Sims, R. and Kirchner, N., "Contribution of renewables to energy security." IEA Information Paper (2007).
- [29] Karlsson, P. and Svensson, J., DC bus voltage control for a distributed power system, IEEE Trans. Power Electron., vol. 18, no. 6, pp. 1405-1412, Nov. 2003.
- [30] Lu, X.; Sun, K.; Guerrero, J. M.; Vasquez, J. C.; Huang, L. and Teodorescu, R., SoC-based droop method for distributed energy storage in dc Microgrid applications, in Proc. IEEE Int. Symp. Ind. Electron.(ISIE), 2012, pp. 1640-1645.
- [31] Ferreira, R. A. F.; Braga, H. A. C.; Ferreira, A. A. and Barbosa, P. G., Analysis of voltage droop control method for dc Microgrids with Simulink: modeling and simulation, in Proc. 10th IEEE/IAS Int. Conf. Ind. Appl. (INDUSCON), 2012, pp. 16.
- [32] Lopes, J. A. P.; Moreira, C. L. and Madureira, A. G., Defining control strategies for Microgrids islanded operation, IEEE Trans. Power Syst., vol. 21, no. 2, pp. 916-924, May 2006.
- [33] Kundur, P., Power System Stability and Control, McGraw-Hill Education, (1994).
- [34] Hornik, T.; Zhong, Q. C., "A Current-Control Strategy for Voltage-Source Inverters in Microgrids Based on H^∞ and Repetitive Control," Power Electronics, IEEE Transactions on , vol.26, no.3, pp.943-952, March 2011.

- [35] Lennart, A.; Lindberg, L., "Inner phase angle control of voltage source converter in high power applications," Power Electronics Specialists Conference, 1991. PESC '91 Record., 22nd Annual IEEE , vol., no., pp.293,298, 24-27 Jun 1991.
- [36] Rodriguez, J.; Pontt, J.; Silva, C.A; Correa, P.; Lezana, P.; Cortes, P.; Ammann, U., "Predictive Current Control of a Voltage Source Inverter," Industrial Electronics, IEEE Transactions on , vol.54, no.1, pp.495,503, Feb. 2007.
- [37] Abu-Rub, H.; Guzinski, J.; Krzeminski, Z.; Toliyat, H. A, "Predictive current control of voltage source inverters," Industrial Electronics Society, 2001. IECON '01. The 27th Annual Conference of the IEEE , vol.2, no., pp.1195,1200 vol.2, 2001.
- [38] Lin, C.T., "Structural controllability." Automatic Control, IEEE Transactions on 19.3 (1974): 201-208.
- [39] Vandoorn, T., et al. "A voltage-source inverter for microgrid applications with an inner current control loop and an outer voltage control loop." International Conference on Renewable Energies, and Power Quality (ICREPQ09). 2009.
- [40] Ford, G. W. and Uhlenbeck, G. E., "Combinatorial Problems in the Theory of Graphs III." Proc. Nat. Acad. Sci. USA 42, 529-535, 1956.
- [41] Allag, T.; Das, T., "Robust Control of Solid Oxide Fuel Cell Ultracapacitor Hybrid System," Control Systems Technology, IEEE Transactions on , vol.20, no.1, pp.1,10, Jan. 2012.
- [42] Das, T.; Snyder, S., "Adaptive Control of a Solid Oxide Fuel Cell Ultra-Capacitor Hybrid System," Control Systems Technology, IEEE Transactions on , vol.21, no.2, pp.372,383, March 2013.

- [43] Greenwell, W.; Vahidi, A, "Predictive Control of Voltage and Current in a Fuel Cell-Ultracapacitor Hybrid," *Industrial Electronics, IEEE Transactions on* , vol.57, no.6, pp.1954,1963, June 2010.
- [44] Drobia, A; Jose, P.; Mohan, N., "An approach to connect ultracapacitor to fuel cell powered electric vehicle and emulating fuel cell electrical characteristics using switched mode converter," *Industrial Electronics Society, 2003. IECON '03. The 29th Annual Conference of the IEEE* , vol.1, no., pp.897,901 vol.1, 2-6 Nov. 2003.
- [45] Single 9-a high-speed low-side mosfet driver with enable.
<http://www.ti.com/lit/ds/slusa13b/slusa13b.pdf>.
- [46] <http://greenlightnational.com/why-colleges-are-big-believers-in-microgrids/>
- [47] Majumder, R.; Ghosh, A; Ledwich, G.; Zare, F., "Angle droop versus frequency droop in a voltage source converter based autonomous microgrid," *Power & Energy Society General Meeting, 2009. PES '09. IEEE* , vol., no., pp.1,8, 26-30 July 2009.
- [48] Slootweg, J.G.; Kling, W.L., "Impacts of distributed generation on power system transient stability," *Power Engineering Society Summer Meeting, 2002 IEEE* , vol.2, no., pp.862,867 vol.2, 25-25 July 2002.
- [49] Donnelly, M.K.; Dagle, J.E.; Trudnowski, D.J.; Rogers, G.J., "Impacts of the distributed utility on transmission system stability," *Power Systems, IEEE Transactions on* , vol.11, no.2, pp.741,746, May 1996.
- [50] Ganguly, S., Sahoo, N. C. and Das, D., "A novel multi-objective PSO for electrical distribution system planning incorporating distributed generation." *Energy Systems* 1.3 (2010): 291-337.

- [51] Carvalho, P. M S; Correia, Pedro F.; Ferreira, L.AF., "Distributed Reactive Power Generation Control for Voltage Rise Mitigation in Distribution Networks," *Power Systems, IEEE Transactions on* , vol.23, no.2, pp.766,772, May 2008.
- [52] Masters, C. L., "Voltage rise: the big issue when connecting embedded generation to long 11 kV overhead lines," *Power Engineering Journal* , vol.16, no.1, pp.5,12, Feb. 2002.
- [53] Bollen, M. H J; Sannino, A, "Voltage control with inverter-based distributed generation," *Power Delivery, IEEE Transactions on* , vol.20, no.1, pp.519,520, Jan 2005.
- [54] Jancke, G.; Fahlen, N.; Nerf, O., "Series capacitors in power systems," *Power Apparatus and Systems, IEEE Transactions on* , vol.94, no.3, pp.915,925, May 1975.
- [55] Iliceto, F.; Cinieri, E., "Comparative analysis of series and shunt compensation schemes for AC transmission systems," *Power Apparatus and Systems, IEEE Transactions on* , vol.96, no.6, pp.1819,1830, Nov. 1977.
- [56] Li, Y. W.; Kao, C. N., "An Accurate Power Control Strategy for Power-Electronics-Interfaced Distributed Generation Units Operating in a Low-Voltage Multibus Microgrid," *Power Electronics, IEEE Transactions on* , vol.24, no.12, pp.2977,2988, Dec. 2009.
- [57] Zhou, H.; Bhattacharya, T.; Duong .T; Siew, T.S.T.; Khambadkone, AM., "Composite Energy Storage System Involving Battery and Ultracapacitor With Dynamic Energy Management in Microgrid Applications," *Power Electronics, IEEE Transactions on* , vol.26, no.3, pp.923,930, March 2011.
- [58] Hines, P.; Talukdar, S., "Reciprocally altruistic agents for the mitigation of cascading failures in electrical power networks," *Infrastructure Systems and Services: Building*

- Networks for a Brighter Future (INFRA), 2008 First International Conference on , vol., no., pp.1,6, 10-12 Nov. 2008.
- [59] McArthur, S.D.J.; Davidson, E.M.; Catterson, V.M.; Dimeas, AL.; Hatziargyriou, N.D.; Ponci, F.; Funabashi, T., "Multi-Agent Systems for Power Engineering Applications Part I: Concepts, Approaches, and Technical Challenges," *Power Systems, IEEE Transactions on* , vol.22, no.4, pp.1743,1752, Nov. 2007.
- [60] Dorfler, F.; Jovanovic, M.R.; Chertkov, M.; Bullo, F., "Sparse and optimal wide-area damping control in power networks," *American Control Conference (ACC), 2013* , vol., no., pp.4289,4294, 17-19 June 2013.
- [61] Yih-Fang. H; Werner, S.; Jing Huang; Kashyap, N.; Gupta, V., "State Estimation in Electric Power Grids: Meeting New Challenges Presented by the Requirements of the Future Grid," *Signal Processing Magazine, IEEE* , vol.29, no.5, pp.33,43, Sept. 2012.
- [62] <http://www.energy.gov/>
- [63] Takahashi, I; Noguchi, T., "A New Quick-Response and High-Efficiency Control Strategy of an Induction Motor," *Industry Applications, IEEE Transactions on* , vol.IA-22, no.5, pp.820,827, Sept. 1986.
- [64] Guo, Y., Hill, D. J., and Wang, Y., "Nonlinear decentralized control of large-scale power systems," *Automatica*, 36(9), 1275-1289, 2000.
- [65] Ugrinovskii. V and Pota. H, "Decentralized control of power systems via robust control of uncertain markov jump parameter systems," In *Proceedings of 43rd IEEE Conference on Decision and Control*, pages 35033508, December 2004.
- [66] Aquino-Lugo. A, "Distributed and decentralized control of the power grid," PhD thesis, University of Illinois at Urbana-Champaign, 2011.

- [67] Tuladhar, A.; Jin, K.; Unger, T.; Mauch, K., "Parallel operation of single phase inverter modules with no control interconnections," Applied Power Electronics Conference and Exposition, 1997. APEC '97 Conference Proceedings 1997., Twelfth Annual , vol.1, no., pp.94,100 vol.1, 23-27 Feb 1997.
- [68] Hines, P.; Talukdar, S., "Reciprocally altruistic agents for the mitigation of cascading failures in electrical power networks," Infrastructure Systems and Services: Building Networks for a Brighter Future (INFRA), 2008 First International Conference on , vol., no., pp.1,6, 10-12 Nov. 2008.
- [69] Haddad, M.M.; Hui, Qing; Chellaboina, V.; Nersesov, S.G., "Hybrid decentralized maximum entropy control for large-scale dynamical systems," American Control Conference, 2006 , vol., no., pp.6 pp.,, 14-16 June 2006.
- [70] Ramakrishna, A.; Viswanadham, N., "Decentralized control of interconnected dynamical systems," Decision and Control including the Symposium on Adaptive Processes, 1980 19th IEEE Conference on , vol., no., pp.538,543, 10-12 Dec. 1980.
- [71] Bakule. L, Decentralized control: An overview. Annual Reviews in Control, 32(1):87-98, 2008.